CANADIAN THESES

THÈSES CANADIENNES

NOTICE

The quality of this microfiche is heavily dependent upon the quality of the original thesis submitted for microfilming. Every effort has been made to ensure the highest quality of reproduction possible.

If pages are missing, contact the university which granted the degree.

Some pages may have indistinct print especially if the original pages were typed with a poor typewriter ribbon or if the university sent us an inferior photocopy.

Previously copyrighted materials (journal articles, published tests, etc.) are not filmed.

Reproduction in full or in part of this film is governed by the Canadian Copyright Act, R.S.C. 1970, c. C-30.

AVIS

La qualité de cette microfiche dépend grandement de la qualité de la thèse soumise au microfilmage. Nous avons tout fait pour assurer une qualité supérieure de reproduction.

S'il manque des pages, veuillez communiquer avec l'université qui a conféré le grade.

La qualité d'impression de certaines pages peut laisser à désirer, surtout si les pages originales ont été dactylographiées à l'aide d'un ruban usé ou si l'université nous a fait parvenir une photocopie de qualité inférieure.

Les documents qui font déjà l'objet d'un droit d'auteur (articles de revue, examens publiés, etc.) ne sont pas microfilmés.

La reproduction, même partielle, de ce microfilm est soumise à la Loi canadienne sur le droit d'auteur, SRC 1970, c. C-30.

THIS DISSERTATION HAS BEEN MICROFILMED EXACTLY AS RECEIVED

LA THÈSE A ÉTÉ MICROFILMÉE TELLE QUE NOUS L'AVONS REÇUE

Static and Dynamic Balancing of High Speed Fibre Composite Rotors

by

Marc Pierre Marchand

A thesis
presented to the University of Ottawa
in fulfillment of the
thesis requirement for the degree of
Master of Applied Science
in
Mechanical Engineering

ISBN 0-315-33358-8

UNIVERSITÉ D'OTTAWA
UNIVERSITY OF OTTAWA

ACKNOWLEDGMENT

To Dr. R. C. Flanagan, the author expresses his profound appreciation for his valuable support, advice and guidance offered throughout the course of his work. Also, the author wishes to thank Philip Miller and Luc Menard for their personal and professional contributions. Further appreciation is expressed toward the personnel of the Department of Mechanical Engineering.

This research was supported by the National Research Council of Canada under contracts OSU80-00043, OSU82-00422 and OST84-00459 and in part by the Natural Sciences and Engineering Research Council of Canada under grants A1638 AND G1009.

All composite hub materials (SMC and S2-L) used for final rotors (FW1 and FW2), prototype rotor and material tests were supplied by Owens-Corning Fiberglass Corporation, Granville, Ohio.

ABSTRACT

The goals of this project were to ensure the proper interpretation of the dynamic responses of high speed, high energy density fibre composite rotors under dynamic spin test conditions and to verify each rotor's capacity in maintaining acceptable levels of vibration, at the University of Ottawa spin test facility.

The primary objective was fulfilled by the development of suitable balancing procedures to eliminate all the synchronous forcing functions acting upon the rotating system. Because of the system's inherent strong cross coupling, a special approach to balancing was developed in that the direct application of available dynamic balancing procedures was not effective in achieving a high precision state-of-balance. Further, vectorial compensation within the balancing computations or signal nulling at the source was required to account for the runouts due to the buildup of machining, assembly, misalignment and tilt tolerances of the pendulously mounted rotors. A complete set of high speed rotor dynamic experiments were conducted to assess the effects of each of the above mentioned parameters. This work culminated in a study of rotor retrograde whirl induced by pure moment imbalance and was shown to correlate with classical gyrodynamic theory.

Plagued by subsynchronous vibrations once the imbalances were reduced, an investigation by the author revealed the cause to be related to the squeeze film bushings in the damper unit of the high speed air turbine which were behaving as journal bearings. The hydrodynamic nature of the problem entrained a

multitude of experiments, based on horizontal and vertical hydrodynamic models of journal bearings. The experiments ranged from bearing hole enlargement, bearing materials modification, replacement by roller element bearing to bearing configuration modification, some of which were quite effective in controlling or eliminating the resonant oil whip–dry friction phenomenon.

The final rotor balance evaluation tests revealed that the composite hub rotors experienced some mass shifting or component seating during their first several runs to maximum or design speed. Thereafter they became very stable, repeatable and predictable. On the other hand, however, the metallic hub rotors did not show any such behavior, once balanced they retained that balance. Further, no evidence of mass shifting (or creep) in the wet–filament wound fibre composite rings could be inferred from any of the rotor tests or dynamic experiments.

Thus, from both the balancing and state–of–balance retention points of view, the metallic hub rotors were the most desirable. Due to these characteristics, they were used for all of the high speed rotor dynamic experiments.

TABLE OF CONTENTS

LIST OF FIGURES

LIST OF TABLES

Chapter I
INTRODUCTION

Optimization and performance studies conducted on flywheel hybrid powertrain systems, such as a Heat Engine/ Flywheel/ Continuously Variable Transmission configuration, for vehicle propulsion in urban duty cycles clearly indicated that substantial improvements in fuel economy would result [18,23,25]. Further, a number of prototype vehicles have demonstrated such drives both in the U.S. and Europe. For example, the conversion of a Ford Pinto to an Internal Combustion Engine (Otto)/ Steel Flywheel/ Continuously Variable Transmission propulsion system at the University of Wisconsin demonstrated a 50% improvement in fuel economy. Work is now under progress for a second-generation design aiming at a 100% improvement [12]. The University of Wisconsin effort has proven the concept to be viable and with the advent of fibre composite technology for flywheel rotor construction, the outlook is even brighter. These high-strength, light-weight materials offer two major advantages, namely: high specific energies and safe, even benign, failure modes.

There has been an ongoing research program since the summer of 1979 on high energy density fibre composite rotor design, manufacture and testing at the University of Ottawa department of Mechanical Engineering. Extensive rotor design studies, based on the properties of these relatively unprecedented anisotropic materials, [19,20,37,38,39,40,41], were the mainstay for the establishment of a dynamic spin test facility. Proof testing of rotor components and final rotor assemblies, through actual dynamic loading, was mandatory in

order to determine and correlate the different materials' ultimate strength's and failure modes, as well as to evaluate and assess the different fibre composite flywheels designed as being competitive and troublefree energy storage devices. Such tests require precision balancing and a thorough understanding of dynamic signal analysis and interpretation.

All research was conducted in the high-speed spin-test facility developed for the composite rotor program [32]. This laboratory provides precision rotor dynamic monitor and signal analysis and its layout, equipment and monitoring systems are described in Chapter 2.

A balancing technique was developed and implemented for these flexibly mounted, overhung composite rotors. This task proved to be quite elusive in that conventional rotor balance practice was not effective. This subject, together with a review of balance theory, is presented in Chapter 3.

As mentioned above, an important aspect of the rotor test program was to evaluate rotor dynamic response over its operating speed range. This objective is particularly significant in composite rotor designs in that rotor dynamic instability and/or the loss of rotor balance (mass shifting) has accounted for many, if not most, rotor failures. The root problem lies not only in the high rotational speeds of composite material rotors but also, and primarily, due to their material properties. The high-strengh, moderately-low-modulus composites experience very large radial growth patterns over their operating speed range. Thus, component radial compatibility and mass shifting is an inherent problem and rotor designs/components must account for this. It could be noted that all rotor components and rotors (except metallic simulators) involved in this work employ specially designed radially expanding hubs or shaft attachment systems. Thus, it is necessary to separate (i) drive system induced from (ii) rotor state of

balance induced from (iii) rotor design/behavior induced dynamic response. In this light, interpreting rotor dynamic response signals became, as with balancing (which is integral with this problem), quite elusive. As such, a number of dynamic experiments and system evaluation studies were conducted. This research component is reviewed in Chapters 4 and 5.

The focus of this thesis is on rotor balancing and the problematic dynamic responses encountered. Many researchers in the flywheel field have attested to the different problems encountered in spin testing [2,3,13,31,45,46,47,48,49], precipitating a series of modelling studies of the pendulously mounted rotor configuration [4,7,31,52]. Although a tremendous amount of work was done prior to the selection of the final four fibre composite rotor designs, this thesis shall concentrate on these last four rotors, since they represent the apogee of the research program. More specifically, they are the concluding proof tests of the balancing procedures developed for the "High Energy Density Fibre Composite Flywheel Research Program". This work is presented in Chapter 6 and general conclusions are given in Chapter 7. In summary, the objectives of this thesis are:

1. to establish a high speed, precision balance laboratory;
2. to establish a balance technique effective for high-energy-density fibre composite rotors in a flexible, overhung mount;
3. to assess the dynamic response of such rotors to a known state of balance; and
4. to evaluate each rotors' ability to retain its state of balance throughout its operating speed range and cyclic operation.

Chapter II
SPIN TEST FACILITY REVIEW

An overview of the spin test laboratory, pertinent to this thesis, is given below. The author refers the reader to reference[32] for a complete description of the facility. Figure 2.1 depicts the overall laboratory layout with its prime constituents. Missing from the figure is the automated control and monitoring (ACM) system which is located in the adjacent fuels testing engine laboratory.

The chamber is set up on a vibration isolation pad. Safety features from the layout include: below grade location of the vacuum chamber, flow-through ventilation in the test chamber room and the separate location of the control room.

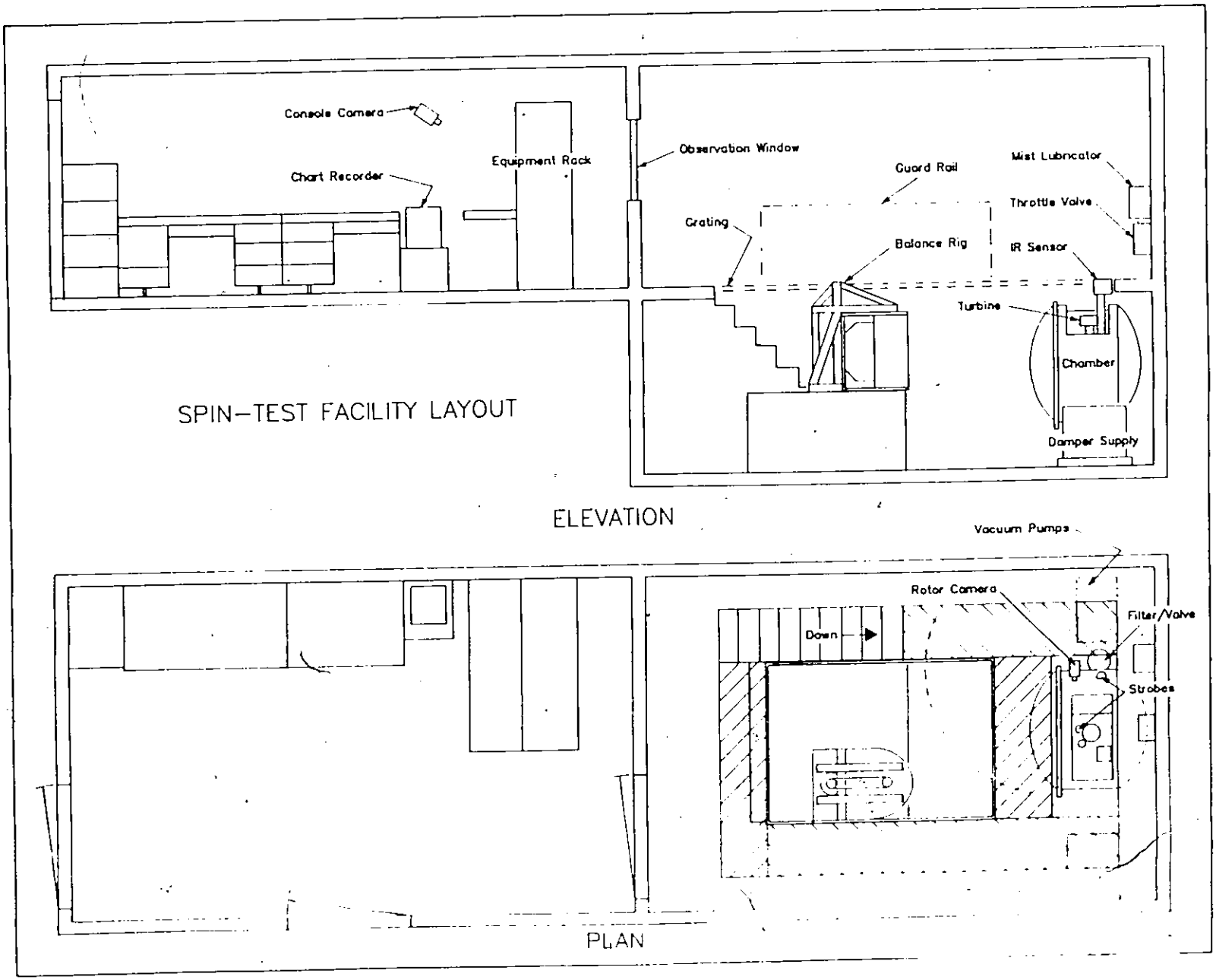

Figure 2.1: Spin Test Facility Layout

2.1 *Test Laboratory*

The heart of the test laboratory is the vacuum chamber where flywheel balancing and high speed dynamic spin tests were performed.

The chamber has a vertically hinged front door with welded in steel containment designed to surround the flywheel once the door is closed. Provision and modifications were made[32] to accommodate equipment required for spin testing, balancing and thorough monitoring of the different dynamic and environmental parameters. The physical rotor drive unit is a 60,000 RPM high-speed 4" bi-directional Barbour Stockwell air turbine, model 2702, with damped drive. Figure 2.2 shows a crossectional view of the turbine.

The test chamber is also equipped with rotor vibration instrumentation, instrumentation feedthroughs, viewing and lighting ports, a temperature monitoring port, vacuum pressure gauge, vacuum pump hookups and air or nitrogen quick purge and controlled bleed hookups.

The chamber, when viewed from above as in Figure 2.3 with the front door closed, features many of the principal components. The turbine occupies the central position and is seen with the drive and brake air supply lines, the damper oil supply and scavenge with thermocouples as well as the bearing mist lubrication hose. Behind it are the instrumentation feedthroughs and to the right is the Modline non-contacting infrared temperature sensor head, series 8000, followed by a Vacuum General CMT capacitance manometer used to measure pressures below 1 Torr. A Granville-Phillips Pirani-type vacuum gauge series 275, for pressures above 1 Torr, is mounted below. The rightmost piece of equipment is a SOL-124 lubricating unit, also shown in Figure 2.4, used to supply oil to the turbine damper section with oil pressure remotely controlled via a DC-motor driven valve.

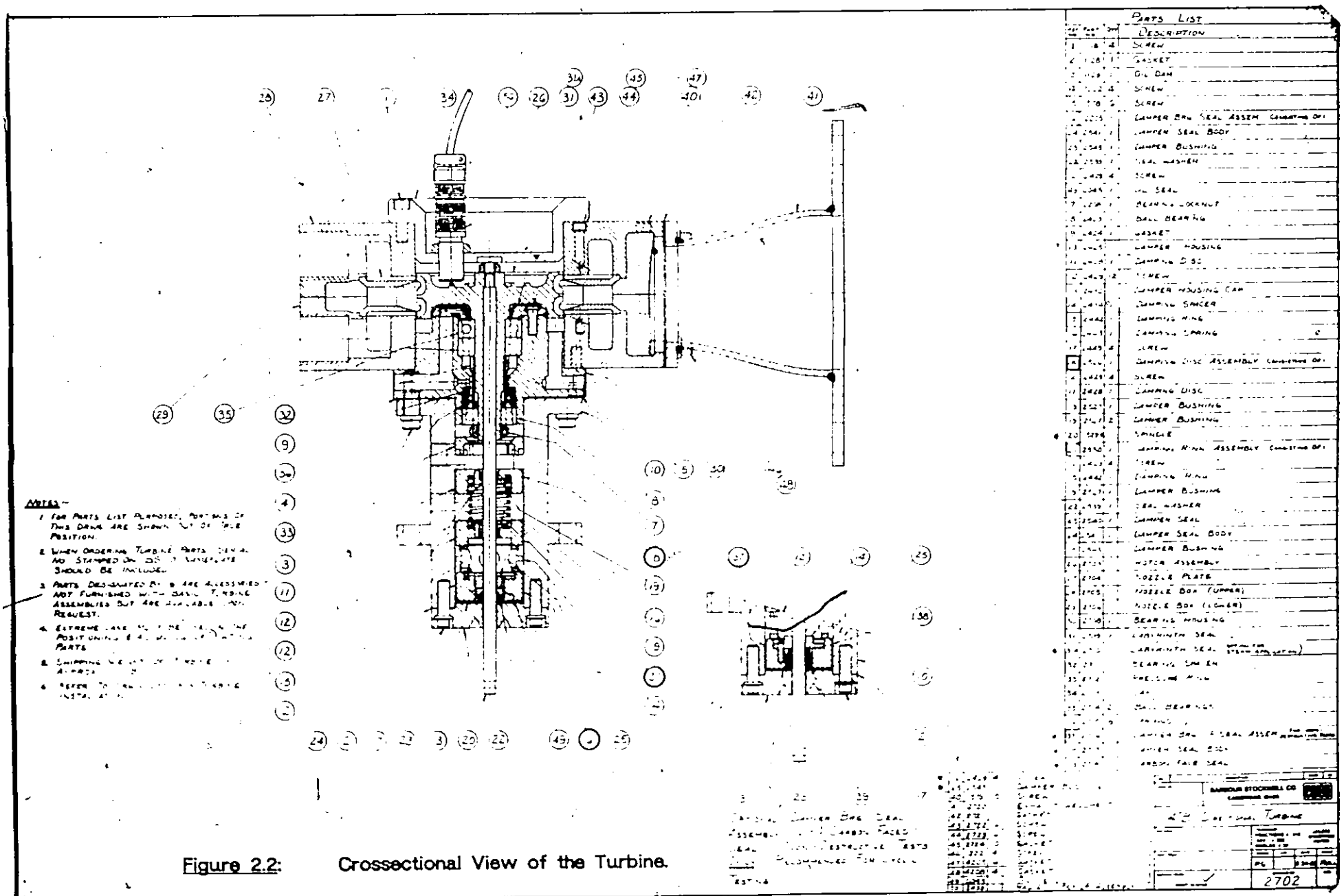

Figure 2.2: Crossectional View of the Turbine.

To the left of the turbine from front to rear is one of the quick purge solenoid valves and the Vacuum General magnetically actuated proportioning valve, model 79-6A, followed by an obliquely mounted Sony SL-5800 camera and one of two Bruel and Kjaer strobe lights. Below is the Edward's inlet dust filter/valve (model ITF 100) which isolates the vacuum pumps from the vacuum chamber, which is shown Figure 2.5 to the right. Finally, on the same lower level as the SOL-124 lubricating unit, but in the left corner of the laboratory, are the vacuum pumps. They are comprised of an Edwards roots blower model EH250, backed by a two stage rotary pump model E2M18. The vacuum pump assembly is shown in Figure 2.5 with the roots booster pump on top.

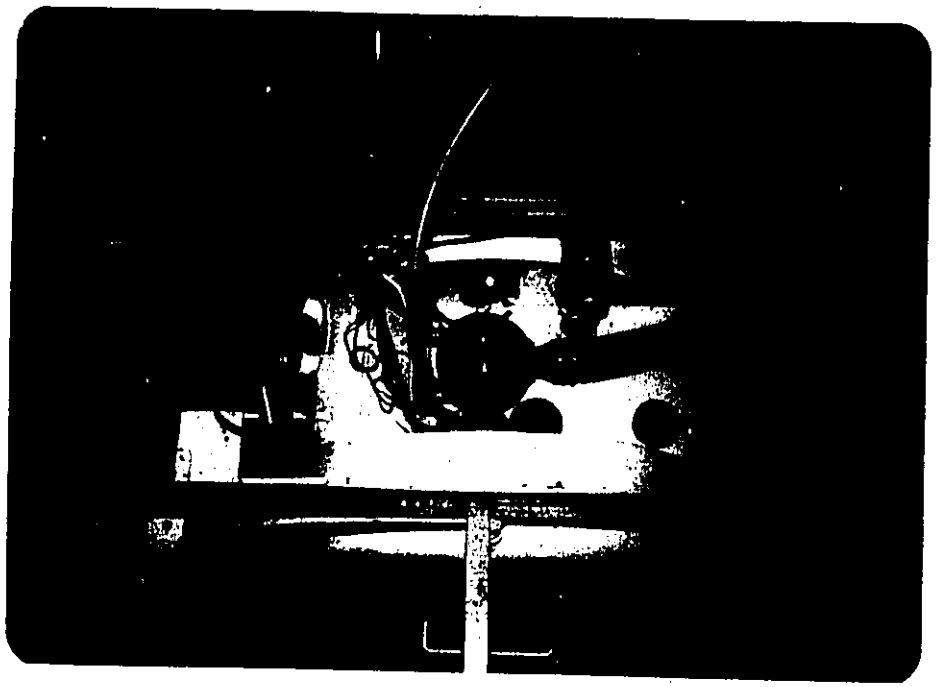

Figure 2.3: Top Outside View of the Vacuum Chamber.

Within the chamber, Figure 2.6 displays the upper and lower catchers which restrict lateral motion of the rotor to 20 and 50 mils (1 mil=0.001 inch).

Figure 2.4: SOL-124 Lubricating Unit.

respectively, as well as the upper and lower probe holders. Each probe holder held two Bentley Nevada non-contacting 5 millimeter proximity probes, series 7200, having an 80 mils linear range between 10 and 90 mils. The probes are mounted at right angles to each other (Figure 2.7) for orbit analysis. A fifth probe, installed above the upper probe holder, called a key phasor probe, provided a once per shaft revolution reference pulse required for phase information, balancing and nonsynchronous vibration analysis.

Figure 2.8 and Figure 2.9 present views of a typical rotor installation in the vacuum chamber, ready for either balancing or testing. LS1, a full sized aluminum simulator [32], is shown pendulously mounted from the nominal 5/16" O.D. turbine high precision quill shaft, as were all the rotors tested. The upper and lower probe holders, as well as the upper and lower catchers, are visible. The probes are rated to 600,000 RPM for dynamic monitor and were calibrated, against the probe target materials used, in the laboratory.

Figure 2.5: Vacuum Pumps and Inlet Dust Filter.

The instrumentation and control wiring were carried to the control room via an instrumentation cable tray.

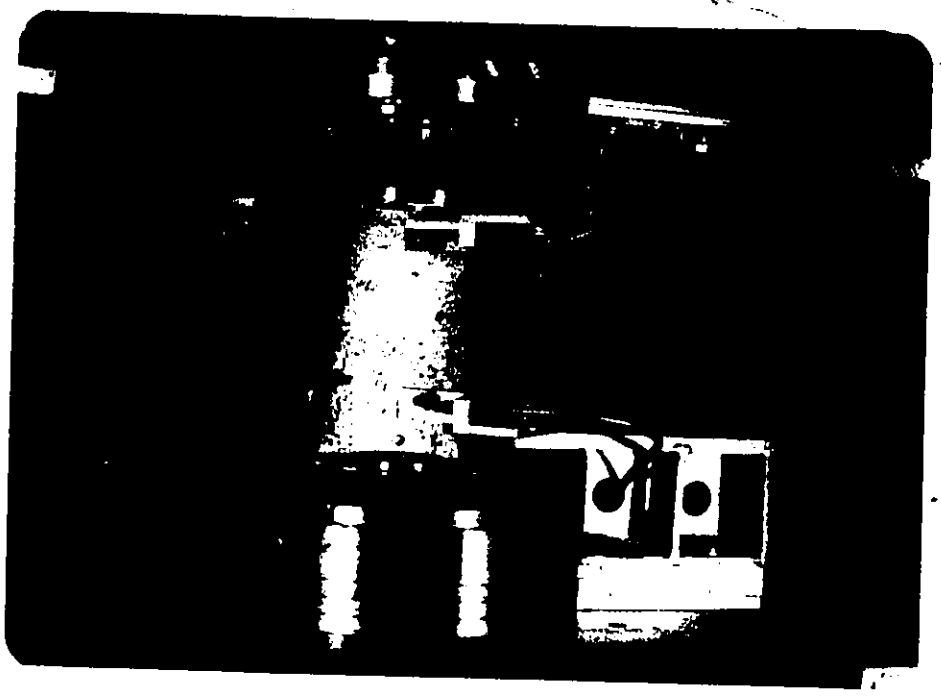

Figure 2.6: Inside View of the Vacuum Chamber.

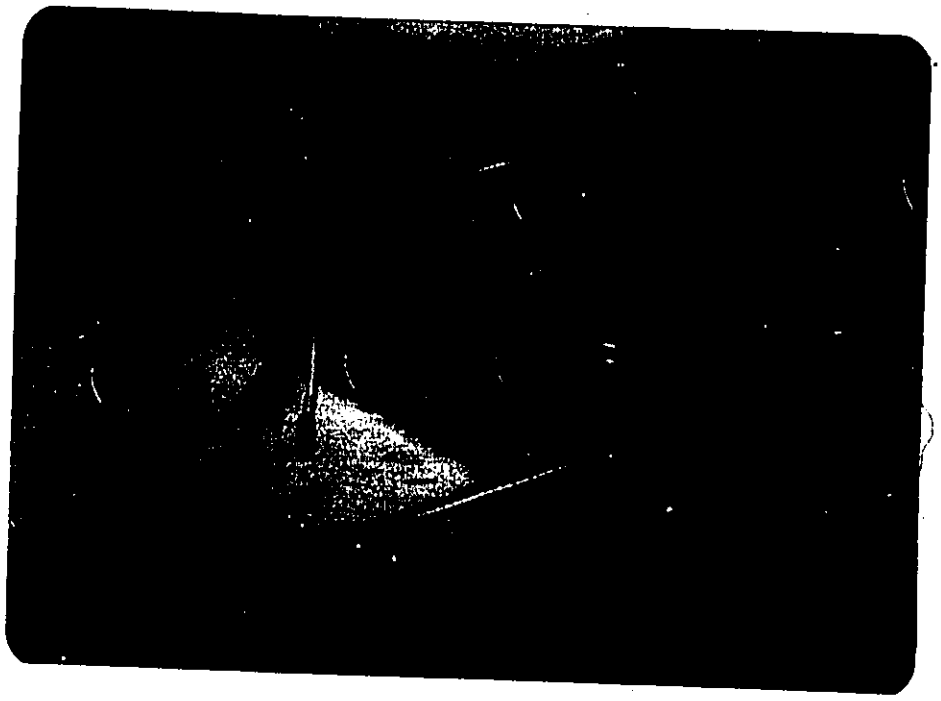

Figure 2.7: Lower Probe Holder.

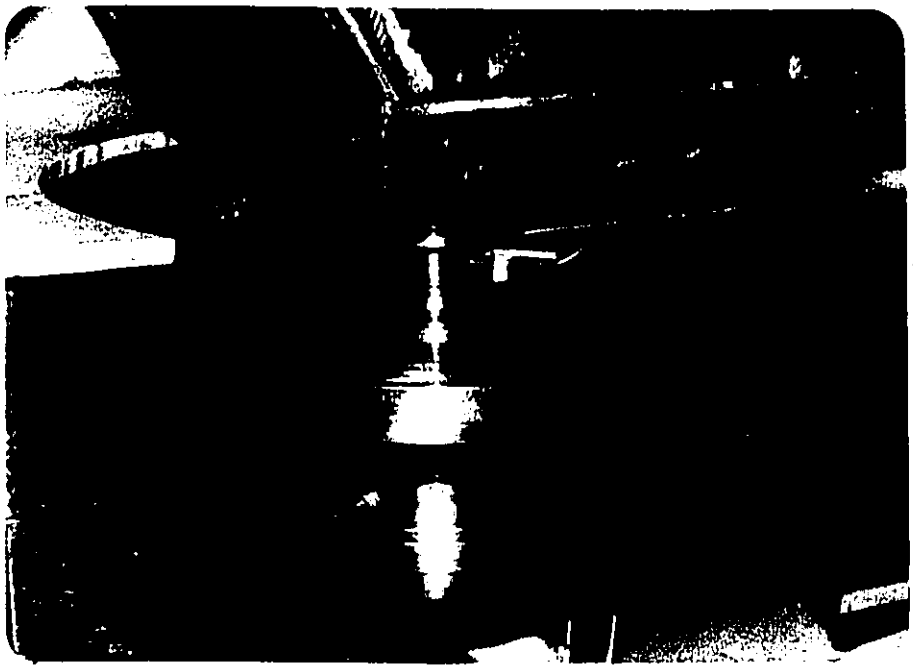

Figure 2.8: LS1, Top View. Full Size Aluminum Simulator Installed in the Vacuum Chamber.

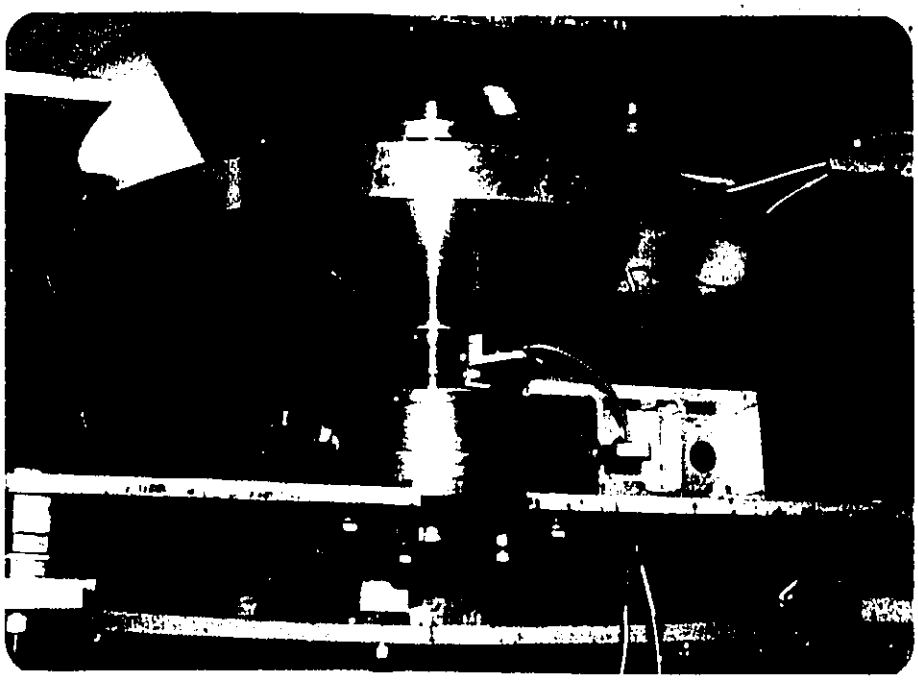

Figure 2.9: LS1, Bottom View. Full Size Aluminum Simulator Installed in the Vacuum Chamber.

2.2 *Control Room*

The monitoring, data processing and control equipment were rack mounted in the control room as shown in Figure 2.10. In addition to the rack mounted equipment, there were a Gould four channel thermal strip chart recorder series 2400 with two thermocouple amplifiers (not shown), an ONO SOKKI mini FFT analyzer system (right) and the ACM system located in the adjacent fuels testing engine laboratory.

Figure 2.10: Console.

2.2.1 *Left Console*

The left console held, from top to bottom (Figure 2.10); a turbine air supply pressure gauge, damper oil inlet and outlet temperature displays, rotor temperature display, vacuum pressure display and pressure controller, main control panel and video recorder. The main control panel was comprised of: (i)

interlocked vacuum pump power switches keeping the booster pump from operating without the rotary pump; (ii) turbine mist lubrication power switch; (iii) turbine damper power switch; (iv) turbine manual or computer controlled drive and brake air supply switches; (v) vacuum isolation valve control switch and (vi) vacuum tank quick purge switches. Status annunciator lights accompanied each of the controls. The video recorder provided a complete audio–video record of each test. This included a continuous audio (mixed) of both the control room commentary plus the test chamber/rotor sounds and a continuous video. The video used a splitter and a three–camera system which included either rotor 'close–up' or rotor general view plus a continuous dynamic/RPM display.

2.2.2 Center Console

The center console consisted, from top to bottom, (Figure 2.10 on page 14) of a speaker panel with a Sony mini–video camera monitor relaying damper pressure settings. Below was a six channel NEC SAN–EI 8K20 series thermal strip chart recorder which logged the following data: filtered and direct vibration signals, RPM, chamber pressure and damper oil inlet and outlet temperatures. Located in this console below the chart recorder was the Barbour Stockwell turbine drive–control panel with overspeed shutoff and throttle settings followed by the Bruel and Kjaer type 4911 motion analyzer driving the two Bruel and Kjaer strobe lights for flywheel illumination in the chamber. The bottom panel held camera power switches, a VIVCON industries V27SP inserter/splitter, a camera selector switch, damper pressure control switch and vibration monitor reset switch.

2.2.3 Right Console

The top panel of the right console (Figure 2.10 on page 14) contained vibration monitor power and select switches, annunciator lights and the auto sweep box for the Bently Nevada Digital Vector Tracking Filter (DVF-2).

Beneath was the Bently Nevada vibration monitor, series 9000, supplying power to the proximitors and monitoring the direct vibration signals from the X-Y probes inside the chamber. The monitor had presettable vibration levels for alert and danger conditions within its 0 to 20 mils range. After three seconds of each preset condition, relays would be activated to switch on annunciator lights or shut down some equipment, such as the main air solenoid, cutting off drive air to the turbine.

Beneath the vibration monitor was the DVF-2 displaying either filtered, unfiltered or notched vibration amplitudes in mils or micrometers, phase angle in degrees and rotor speed in RPM. The DVF-2 also featured a null module for nulling out initial runout vectors by summing corrective X and Y components into the filters, plus simultaneous X-Y-Y plotter outputs for in-phase and quadrature to produce polar (Nyquist) plots for each channel. This unit had a 100 to 100,000 RPM operating range. The DVF-2 can be used to produce spectral (cascade) and Bode (vibration amplitude vs RPM) plots. However the ONO SOKKI mini FFT analyzer system was used extensively for signal analysis, thus, the DVF-2 was used for balancing and providing DC signals to the thermal chart recorders and the ACM system.

A Tektronix oscilloscope was rack mounted beneath the DVF-2 and displayed either direct or filtered X and Y vibration signals or rotor orbit patterns. In addition, a Polaroid scope camera was available to take permanent records of the different dynamic phenomena encountered. The last item was a

video-monitor used for displaying selected views of the spinning flywheels in conjunction with the DVF-2 LED. display via the VIVCON video splitter.

On the far right, set on a cart, was the ONO SOKKI CF-920 mini FFT analyzer system with active and disk storage capacity. Power spectral analysis was performed using this unit instead of the DVF-2 - auto sweep box configuration.

2.3 *Automated Control and Monitoring*

The ACM system shown schematically in Figure 2.11 accomplished data acquisition, monitoring and control of the spin testing events.

The Lecroy 8212 digitizer (100 KHZ) card converted the analog filtered amplitudes, phases and RPM signals which were then analyzed and stored on floppy disk by a Digital LSI 11/23 mini computer.

An HP 1000 mini computer later transferred the acquired data (amplitude and phase from each plane, RPM and elapsed time) from the floppy disk onto the AMDHAL mainframe computer. Spectral data from the Ono Sokki mini FFT analyzer was also transferred via the HP.

The control software activated either the drive or brake solenoid to the turbine through a Kinetic Systems 3080 output register.

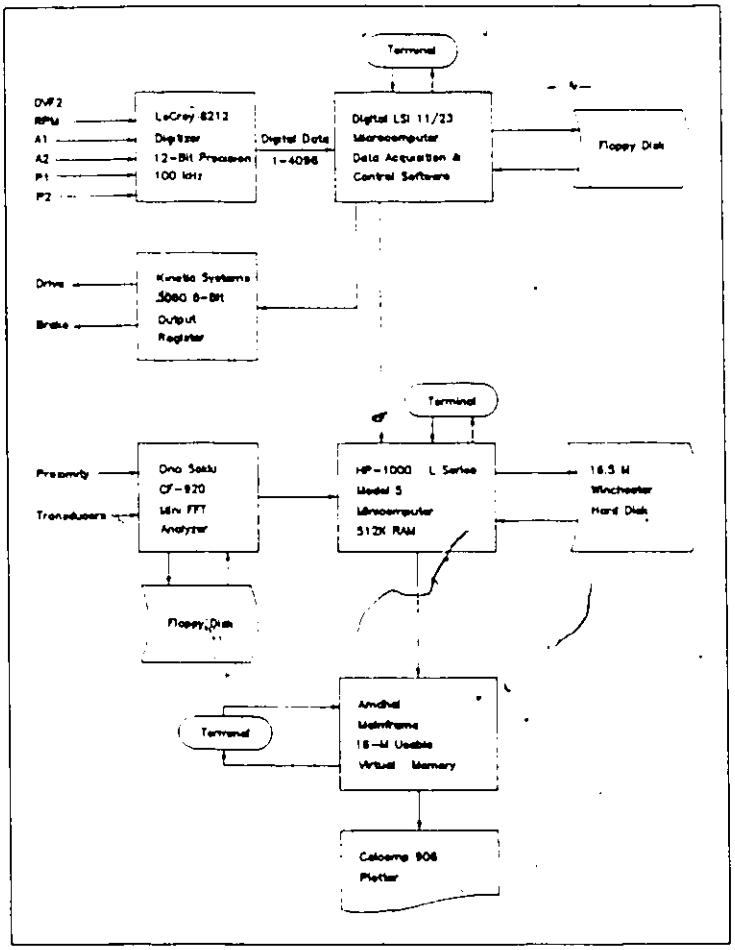

Figure 2.11: Automated Control and Monitoring Layout (ACM).

Chapter III
BALANCING

In their survey on acceptable residual specific imbalance, Muster and Flores [35] recognized the difficulties encountered in the field of balancing when they observed that "achieving better balance in rotors is primarily an art". In this research, the difficulties encountered in determining which balancing methods and techniques to use, which rotor rotational speed to balance at, and at what point the procedures should be applied to the rotors being manufactured all support Muster and Flore's observation. In trying to eliminate all synchronous forcing functions acting on a rotating element through balancing, the balancing engineer will likely be facing other problems related to nonsmooth operation. For example, misalignment, shaft deflection, aerodynamic and hydrodynamic effects, etc., are common and one cannot take a casual approach to applying known balancing methods in the field. Each system requires diligence and study in order to devise and select the proper procedures to balance rotating machines.

These facts make balancing a fundamental engineering concern from design through assembly and operation of rotating machine. Failing to consider the importance of balancing early in a design might result in delaying or even halting research and development work involved with rotating machinery. As discussed in chapter 1, this is particularly true of composite material rotors, an important fact which ultimately lead the second M.A.N. Neue Technologie flywheel research program, in 1980[1] to failure.

[1] From a personal communication to Philip Miller by Gunter Besel of M.A.N Neue Technologie, dated October 16, 1985

3.1 *Balancing Methods and Techniques*

There are two major methods available for flexible shaft rotor balancing, namely; the Modal Balancing Method and the more recent Influence Coefficient Method, the latter technique being applicable to rigid shaft rotor balancing as well. Further, a unified approach is under development where features from both methods are being incorporated[24].

3.1.1 Modal Balancing Method

The modal approach requires knowledge of a rotor's principal modes of vibrations. These can be calculated by analytical methods such as that of Mykelestad (lumped masses connected by massless beam sections), or determined experimentally thus automatically incorporating all the system's dynamic properties and characteristics within the rotor actual modal shapes. An advantage of the latter method is that all the modes of vibration concerned can be corrected for without hindering the corrections made for lower modes provided that the modal effects from higher modes do not alter the dynamic response of the lower modes [5,24]. This method applies to systems having clear and separate modal shapes such as high speed turbomachinery and other high speed machinery operating in their flexible region. Relative flexibility between balance planes is therefore required. A paper by R.E.D. Bishop [5] and a report by P.Y. Kim entitled "Review of Flexible Shaft Balancing Techniques" [24] provide simple and descriptive examples on the Modal Balancing Method.

The fibre composite energy storage rotors, by design, allow a maximum of two balance correction planes which are, in turn, restricted in their axial location and relative positions. Thus, the modal balancing technique is not applicable to these rotors.

3.1.2 Influence Coefficient Method

For the composite rotors, the influence coefficient method was used by adapting the method to the system's dynamic characteristics. The method can best be described by example. Thus, the following discussion presents the method as it would be applied to a two-plane (dynamic) rotor balance problem.

The dynamic responses, A1 and A2, of a rotating machine are vectors having magnitude (displacement, velocity or acceleration) and orientation (phase) with respect to a reference mark on the rotor. By assuming the responses to be the resultant effect of imbalances within the rotor, where I1=imbalance in the first plane and, I2=imbalance in the second plane, the following two equations can be stated.

- $A1 = R(1,1)*I1 + R(1,2)*I2$ (1)
- $A2 = R(2,1)*I1 + R(2,2)*I2$ (2)

R(i,j) are complex functions of the dynamic characteristics of the system and depend strongly on the rotor speed as well. It could be noted that this method assumes an orthogonal (linear) response due to imbalance, thus:

1. R(1,1)=response vector at plane 1 to an imbalance force in plane 1.
2. R(1,2)=response vector at plane 1 to an imbalance force in plane 2.
3. R(2,1)=response vector at plane 2 to an imbalance force in plane 1.
4. R(2,2)=response vector at plane 2 to an imbalance force in plane 2.

To determine the value of the complex functions called "influence coefficients", calibration or trial weight runs must be performed as part of the balancing procedure. These trial weight runs are performed at the same speed at which the "as is" data, A1 and A2, are obtained, namely the balance speed.

Temporarily placing a trial weight (TW1) in the first plane of balance and recording its mass and angular location on the rotor, the modified dynamic responses, B(1,1) & B(2,1), are recorded at balance speed, where:

1: B(1,1)=modified dynamic response in plane 1 with TW1 in place.

2. B(2,1)=modified dynamic response in plane 2 with TW1 in place.

Hence, the following equations result.

- $B(1,1) = R(1,1)*(I1+TW1) + R(1,2)*I2$ (3)
- $B(2,1) = R(2,1)*(I1+TW1) + R(2,2)*I2$ (4)

Now removing TW1, and placing a trial weight TW2 in the second plane of balance and recording its mass and angular location will yield two more modified dynamic responses, B(1,2) & B(2,2), at balance speed.

1. B(1,2)=modified dynamic response in plane 1 with TW2 in place.

2. B(2,2)=modified dynamic response in plane 2 with TW2 in place.

Thus, the last two independent equations can be derived.

- $B(1,2) = R(1,1)*I1 + R(1,2)*(I2+TW2)$ (5)
- $B(2,2) = R(2,1)*I1 + R(2,2)*(I2+TW2)$ (6)

With the calibration or trial weight procedure now completed, six independent equations are available to solve for the six unknowns, namely: R(1,1) R(1,2) R(2,1) R(2,2) and most importantly, the imbalances I1 & I2.

The concept described above can be applied to virtually any number of planes from single plane (static) balancing[22,33] through multiplane balancing[26,51] and even multiplane-multispeed balancing (least-squares procedure)[14,51].

3.2 Application of Balancing Theory

The dynamic balancing procedure demonstrated in section 3.1.2 should, in theory, be effective independent of the imbalance distribution within the rotor. However, the direct application of this method was ineffective in correcting the combination of static and dynamic imbalances found on the pendulously mounted

fibre composite rotors being tested. The "black box" approach of the influence coefficient method is its main drawback.

Pendulously mounted rotors exhibit large cross-coupling effects between balance planes. Cross-coupling effects can be described as a weight's influence on vibration at the opposite end of the rotor, that is the R(1,2) and R(2,1) coefficients involved in the two-plane balancing equations. In this research, it was experimentally verified that if their influence is too great, the rotor must first be adjusted in a manner which leaves a pure couple imbalance which can then be corrected by using the influence coefficient method described above for two plane balancing.

The first step of this procedure involves recording the "as is" vibration readings from each plane observed at balance speed, A1 and A2. A calibration run is done by placing a trial weight (TW) at mid span, its mass and angular position recorded. The modified vibration readings, B1 and B2, are again recorded at balance speed.

The "as is" vectors, A1 and A2, are summed vectorially yielding one vector, "ASUM". The same is done with the modified vectors yielding one vector, "BSUM". Assuming a static imbalance, "I", the following equations can be written.

- ASUM=R*I (7)
- BSUM=R*(I+TW) (8)

Solving for the static imbalance "I", the static component of imbalance on the rotor can now be eliminated leaving a pure couple imbalance. The couple imbalance is then corrected using the two plane influence coefficient balancing approach demonstrated in the previous section.

This two-step approach is based on a method, referred to as the static/couple derivation, described in [33]. It is recommended for balancing

rotors having excessive cross-coupling effects as is commonly found on overhung rotor systems. However, their method differs in the evaluation of the "ASUM" & "BSUM" vectors. Instead of determining the sum of the upper and lower plane vibration response for the working vectors, their values are plotted on polar paper; first for the "as is" and second for trial weight response. The tips are then joined for each pair and the working vectors used for static balancing are determined by tracing vectors from the origin to the mid span of the joining vectors. Figure 3.1 demonstrates this graphical procedure for the evaluation of the "as is" working vector [33].

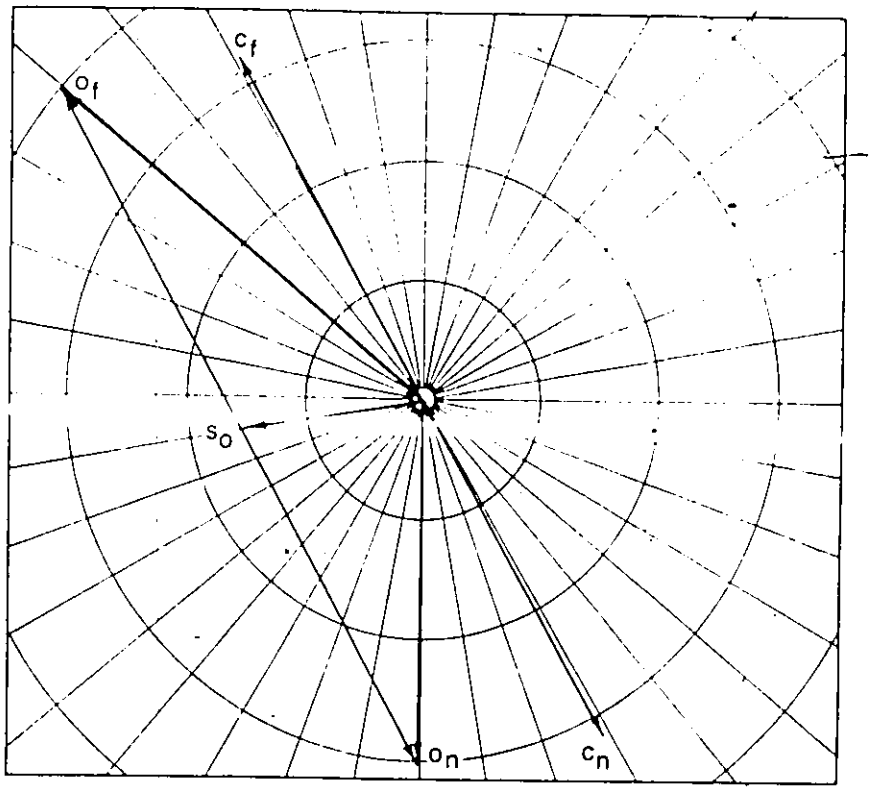

Figure 3.1: Static/Couple Derivation. From Reference (33)

3.3 Residual Imbalance and Trim Balancing

After applying the balance weight(s) to the rotor, there are invariably some residual imbalances remaining. Because each calibration run is time consuming and thus costly, the balancing routines were adapted to allow for the application of previously determined influence coefficient(s) into the after–balance vibration response(s). This required trim balancing to be performed at balance speed, however, the balance engineer could perform trim balancing promptly and efficiently since trial weight runs were bypassed.

3.4 Runout

When measuring rotor dynamic response with non–contacting eddy current proximity probe systems, runout (an apparent motion which becomes superposed on the actual rotor dynamic response) can cause considerable problems. Runout is a combination of electrical and mechanical causes. Electrical runout is a function of the metallurgical properties of the target area which cause perturbations to the magnetic flux path. Such perturbations are naturally interpreted by the proximitor as rotor radial position changes. Mechanical runout is essentially the lack of concentricity of the target area relative to the rotor axis. In any practical rotor system, both electrical and mechanical runout will be present. Considerable care was taken to minimize runout in all of the rotors that were built including component design, machining practice and sequence, high tolerance component aligment and fits as well as target surface grinding and burnishing.

However, each of the pendulously mounted rotors tested unavoidably had some amount of electrical and mechanical runout due to the tilt imparted from the quill shaft, quill shaft–arbour fit and machining and assembly tolerances. In

theory the rotor attitude, as it hangs at rest from the high speed air turbine drive, should be preserved. Thus, the aim of balancing is not to achieve zero vibration readings in each plane monitored at balance speed, but rather to achieve zero rotor dynamic response and to do so, runout must be understood and accounted for. Avoiding consideration of runout will yield apparent low vibration readings at balance speed but large vibration levels outside balance speed. This was observed by other researchers[51]. Experiment FW3A-BD-5 (Chapter 5) investigated the effects of neglecting runout values within the balancing procedures.

From experiments conducted, the only effective runout readings were those taken at the lowest possible speed of rotation at which the vibration signals could be filtered by the DVF-2, namely about 100 RPM. These runout vectors are referred to as slow roll vectors. Static runout readings obtained by rotating the flywheel from angular station to angular station were ineffective for adequate balancing. The slow roll vectors incorporated the drive effects (bearings, seals) as the flywheels rotated while imparting a minimal amount of dynamic forces onto the rotor, which would have altered the characteristic rotor-drive attitude.

Two methods of incorporating the slow roll vectors were tried. The first eliminated the runout vectors, obtained by polar plotting of the filtered slow roll attitude vectors from the DVF-2, in the balancing routines. The degree of difficulty in obtaining precise values from the polar plotting method rendered this approach very undesirable. The second method used built-in nulling circuitry within the DVF-2, thus eliminating the need to compensate within the balancing computations. Both methods were proven effective, the second one requiring much less effort on the part of the balance engineer.

Appendix A contains the listings of the balancing programs used on an HP 41C or 41CV desk calculator.

3.5 Balancing Criteria

The balancing criteria or grades developed through the years are based on experience gained in rotors of various types, sizes and speeds[21,35]. These are recommended balance quality grades, not acceptance specifications, to give indications of how to avoid gross deviances as well as exaggerated or unattainable requirements. These recommended balance quality grades are valid for rigid rotors.

The representation of the state of balance is usually given as specific unbalance (center of gravity displacement). When two plane balancing is considered the recommended value for one plane rotors, obtained from tabulated charts or equations, is halved. For the class of rotor being tested (up to 25000 RPM) at the University of Ottawa, the recommended mean specific unbalance (1 plane) is 0.000004 inches . However, based on Muster and Flores' [35] survey, 68% of the rotors surveyed had residual imbalances no greater than 0.000033" while the residual imbalance for 95% of the rotors surveyed climbed to 0.000250". These are very stringent criteria considering the mass, size and speed of the composite rotors being evaluated. However, the minimum 95% industrial level was observed not only to allow for smooth experiments but to verify the capacity of each flywheel design in maintaining acceptable low vibration levels under actual dynamic loading.

Chapter IV
RESONANT WHIP

As outlined in the introduction, due to the nature of composite rotors, an important R and D requirement was to thoroughly investigate rotor dynamic behavior. Thus, it was imperative that system induced motion, runout and state-of-balance induced motion be completely understood if rotor behavior was to be evaluated from the dynamic response signals. Prior to analyzing state-of-balance cause and effect experiments and case histories of the rotors tested, a particular case of subsynchronous vibration should be reviewed: that of oil whirl or, more specifically, resonant whip.

Each of the rotors tested experienced severe subsynchronous vibration, as long as their state of balance was preserved. Figure 4.1 shows a typical CRT display of an arbour orbit excursion about the center of rotation, magnified 394 times. Each blanked section in the trace indicates the start of one shaft revolution. More than one within an orbit indicates a subsynchronous vibration. The signals were produced by the Bently Nevada 7200 series proximity probes described in the Spin Test Facility Review. The traces display the raw signal, thus electrical and mechanical runouts are included. They do, however, provide excellent feedback on the rotor dynamic response. The blanked sections are produced using the key phasor probe which imparts a once-per-revolution reference pulse to the oscilloscope's Z function.

The orbits displayed toroidal patterns similar to the cusping type motion of a spinning top under the effect of a gravity moment. This similarity clouded an

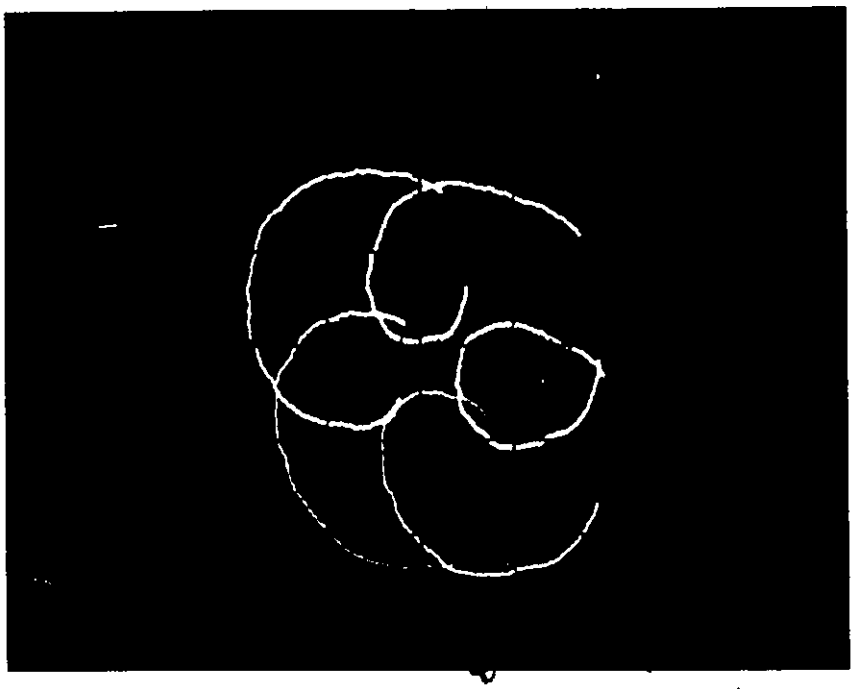

Figure 4.1: Oscilloscope Rotor Orbit Display. Typical Rotor Excursion Due to Resonant Oil Whip, Magnified 394 Times.

understanding of the phenomenon especially when one considers the nature of the flexibly mounted rotors. None-the-less, a careful study traced the problem to the damper unit of the high speed drive turbine which had an inherent resonance giving rise to an oil whirl-dry friction phenomenon.

In 1973 D. Dowson and C.M. Taylor [9] performed a survey on the state of knowledge in the field of bearing influenced rotor dynamics and it was recognized as a complex, highly specialized area of study. The objective of this chapter is to present the observations made on the oil-film bearing influenced rotor dynamics and point to previously recorded observations done by other researchers involved with rotating machines.

Most of the literature on oil-film lubrication influenced rotor dynamics is concerned with half-running-frequency-disturbances, which excites a rotor at about 42 to 48% of running frequency [1,6,10,22,34,42]. This is known to occur when rotors operate as rigid rotors [1,6] and well beyond twice first critical[36].

Resonant whip [36,43,44], however, has a constant frequency of vibration, independent of the shaft speed, usually very close to the first critical of the system. The onset of instability is at shaft speeds just beyond twice first critical. The phenomenon is usually associated with lightly loaded, fully flooded journal bearings, although some researchers have observed resonant whip while maintaining cavitated oil-film conditions [8] where the common belief is that cavitation subdues any already existing whirl [17].

The design of the damper unit is such that the vertical spindle shaft behaved as a journal running through three squeeze film dampers, which in turn act as bearings to the quill shaft, Figure 2.2 on page 7. This machine configuration made it a prime candidate for hydrodynamically induced instabilities such as half-running-frequency-whirl or resonant oil whip [16,43,44] which, unfortunately, was not considered in the numerous models that evaluated this system.

In their work, C.W. Bert and G. Ramanujam[4] developed a linear system analysis to predict the rotor-dynamic characteristics of high-performance, advanced-composite-material flywheel systems pendulously supported in a quill-shaft configuration. Their model corresponded exactly to the University of Ottawa's spin test facility but did not consider resonant oil whip, which proved to be a major concern in rotor dynamics after balancing. The outstanding concern of their analysis was the first forward critical but this was well below the testing range and easily handled with proper balancing and damping.

A. Keith Miller[31] constructed finite element structural models of some of the U.S. rotors tested. He then developed a flywheel–turbine model (Barbour Stockwell model 6100) but neglected the damper assembly. From his experiments, the author observed a hub run–out stabilized into a toroid shape. A clear explanation was not found for the occurrence, consequently it remained a low key issue within the report. Based on our experiments, this behavior could be attributed to the resonant oil whip phenomenon stemming from the damper assembly.

W.T. Thomson[52] presented the steady state whirl–spin relationships for a pendulously supported flywheel with bearing flexibilities, stiff section of shaft and gyroscopic action. It was a more elaborate representation of the basic model developed in Den Hartog's thesis on the gyroscopic effects of a spinning disk located on an overhung shaft [16]. No specific driving system was considered, thus no provisions were taken for the use of journal bearing(s) and the possibility of resonant whip.

T.L.C. Chen and C.W. Bert[7] presented an eight degree of freedom system which considered flexibilities within the rotor. Although the drive modelled was that of a flexible quill shaft and journal bearing type squeeze film damper, no provisions were included for possible resonant oil whip.

From the experiments conducted, instability was observed to increase with damper pressure which corresponded to a greater oil flow through the bearings and with higher damping capacity. This behavior was also observed by Pinkus [43] and Holmes [17]. Further, the onset of the resonant whip was always observed to occur at shaft speeds above two times first critical and persisted well beyond, as long as the rotors' precision state of balance was maintained. However, the frequency of the instability was just above the first critical, at

onset, but then settled at values between two and three times first critical as shaft speed increased, see Figure 4.5. The following system peculiarities of the turbine damper and test speed could be at the source of the differences between what was observed and what other researchers have observed on fluid–film induced instability, as far as the frequency of the resonance is concerned.

1. Some contact (rub) between the journal and bearing had always occurred as was evident from post test inspection.
2. Rotor test speeds reached values of up to 25000 RPM traversing only the first critical speed in the 375–420 RPM range, depending on the rotor. This represents a clear operating range well over 50 times the rotating system's first critical without engaging any higher modes of vibration. This contrasts with that commonly encountered by turbomachinery where more than one critical speed within their operating range is common and where speeds never exceed 2 to 5 times the first critical.
3. The squeeze film bushings used in the damper unit of the turbine drive were unrestrained.

When Poritsky [44] modelled resonant whip using a vertical rotor to eliminate gravity loading, he restricted his work to small displacement theory to maintain a linear system of equations of motion and introduced a radial bearing force (the equivalent of an oil film spring stiffness). His results corresponded to observed resonant whip phenomena. The oil film resilience was assumed to be much greater than that of shaft and to be constant. It is well known today that oil film dynamic characteristics are dependent on many operating parameters, one of which is speed [27] and that they are highly nonlinear [15], especially when

small displacements are no longer representative of the actual phenomenon. Thus the oil film dynamic characteristics between involved parts in the damper need to be clearly defined in order to tune the squeeze film dampers to the rotor bearing system, as is recommended by Gunter [15] and Fleming [11].

Self-exited vibration, including phenomena other than resonant oil whip, impose a restraint on the performance capabilities of rotating machinery. For example, the high pressure turbopumps of the Space Shuttle Main Engine were unstable at speeds approaching twice first critical [11] and could not reach their design speed of 39000 RPM, shutting down the program for six months [10]. The turbopumps continue to be subject to subsynchronous vibration which have prevented NASA from using the shuttle for polar orbits because of the power levels required [10].

In an attempt to resolve this drive system induced rotor dynamic behavior, the air turbine manufacturer was contacted and was aware of the resulting phenomenon and recommended bearing hole enlargements by 0,003 inches diametrically. They had tried replacing the damper bushing, part #2545 in Figure 2.2 on page 7, with teflon and graphite impregnated materials without success.

An "Oilite" (oil impregnated porous bronze) bushing, catalogue # AAM8-11X8, was inserted in the lower damper bushing, where most of the action was known to occur. Under test, the stability was improved until the bearing surface quality had degraded, at 19000 RPM, reducing the bearing's oil feeding capacity and slip characteristics resulting in the reappearance of the resonant oil whip-dry friction phenomena. Thus rub was a contributing factor to the instability once induced hydrodynamically. This test was conducted with the S2L-19 rotor, shown installed in the chamber in Figure 4.2.

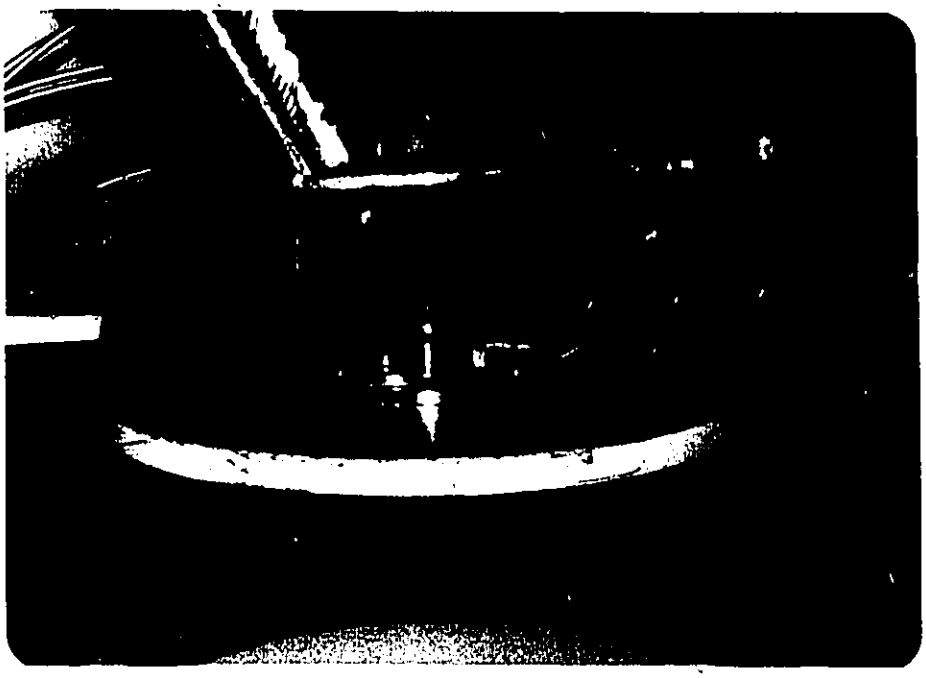

Figure 4.2: Rotor CH-19 installed in the Vacuum Chamber.

The bearing hole enlargement recommended by the manufacturer also proved to be ineffective. While a larger hole would eliminate the hydrodynamics and rubbing involved it would defeat the journal bearing concept of carrying lateral loads and thus overload the oil seal within the lower damper assembly, part #6045 Figure 2.2 on page 7.

A Barden instrument quality ball bearing, catalogue # SR1810SSW3 P103, was then used to carry the lateral loads. The inner race diameter was selected to allow for a sliding fit on the quill shaft. The damper bushing of the lower damper disk was machined accordingly to receive the bearing outer diameter. The test was successful however it was not prolonged, since the bearing was not designed to operate in an oil bath environment. Hence, the test was aborted at the first sign of instability. Post test inspection revealed no evidence of bearing degradation and indeed prolonged testing could have verified the true

capacity of using such a configuration. It is interesting to note that the spin test facility for medium energy density flywheels at the Istituto della Motorizzazione Politecnico di Torino [13] utilized a ball bearing–to–damper configuration to introduce external damping in the spin testing setup. Figure 4.3 reproduced from [13] shows part of their facility with a more detailed view on the external damper (right circle) of the type described above.

Tilting pad journal bearings replacing the damper bushing could be an elegant solution. However, fitting the environment of the damper, shaft size and speed might inhibit such a venture. However, since the maximum level of self excited vibration always remained within tolerable levels and since the phenomena was now well understood and separable from other rotor dynamic behavior, further efforts to eliminate system induced resonant oil–whip rotor response were disbanded. Inadvertently, it was later realized that this phenomena could be used to advantage. The occurrence of a resonant oil whip during a spin test could be used as a yard stick to gauge the load being carried by the damper bearing, giving an indication of the state of balance of the rotor under test. In Figure 4.4 the linear spectrum cascade plots for two independent rotors are compared and demonstrate the resonant oil whip–dry friction phenomena as well as its dependence on bearing load (i.e. as rotor dynamic response –one times amplitude– increases, oil whip disappears). Further, its frequency independence from the shaft running frequency is clearly demonstrated. In Figure 4.5 the resonant oil whip–dry friction amplitude and frequency are plotted against shaft RPM. The frequency and RPM are normalized against the first critical frequency of each respective rotor. The sudden increase in amplitude could be attributed to the "jump phenomenon" associated to squeeze film dampers [15,50].

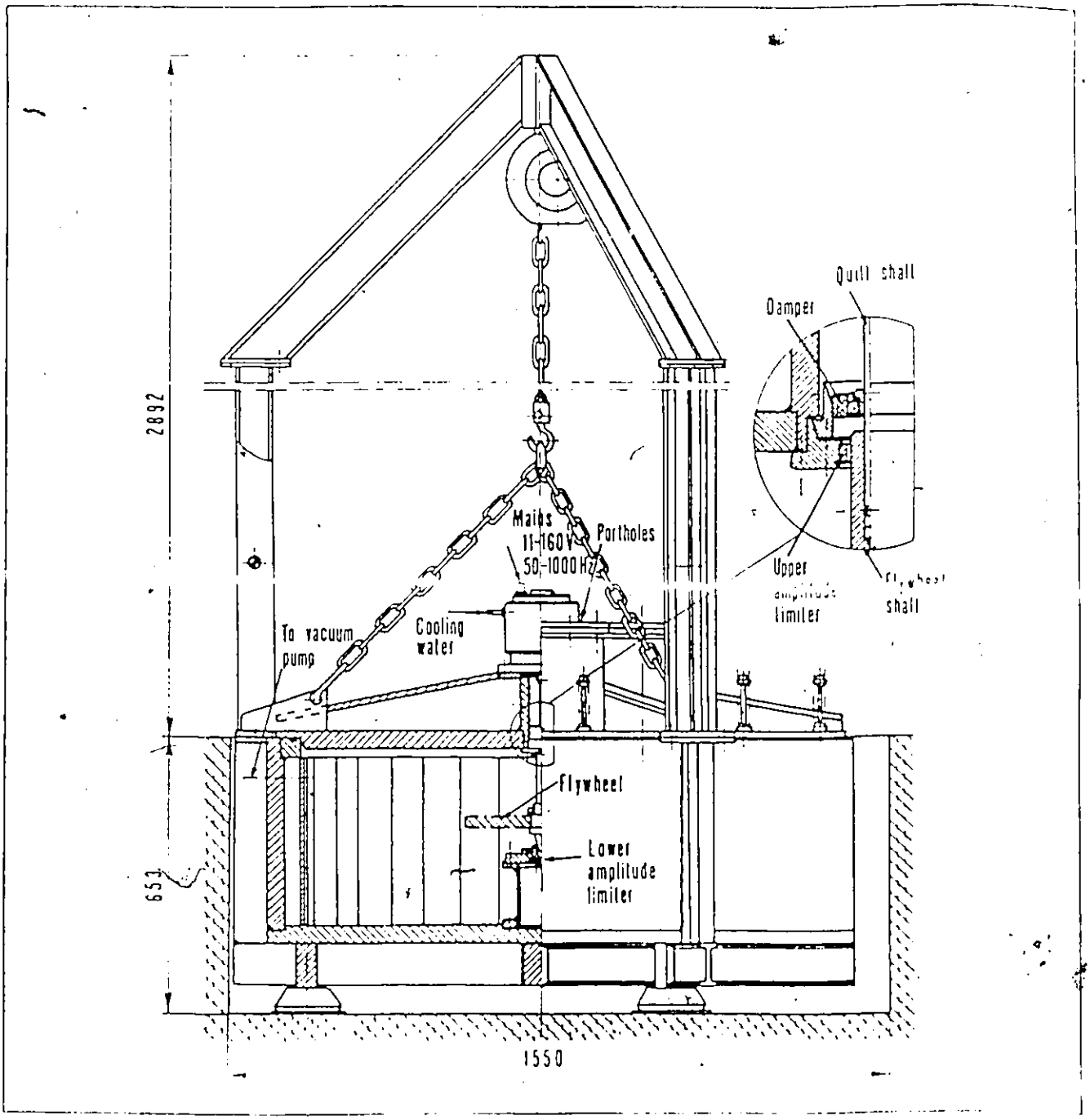

Figure 4.3: Alternate External Damping Method. Spin Test Facility at the Istituto della Motorizzazione -Politechnico di Torino (dimensions in mm).

Although the oil whip amplitude Figure 4.5 was earlier shown to be closely related to rotor one times dynamic response, both rotors do exhibit an almost classical critical speed at about four times normalized shaft speed and at two times normalized whip frequency. Further, as other researchers have observed, onset of whip began at about two times rotor critical shaft speed at a frequency near one time rotor critical. However, the whip frequency, see Figure 4.5, was seen to slowly increase stabilizing at a constant frequency in the order of 2.5 to 3 times rotor critical speed.

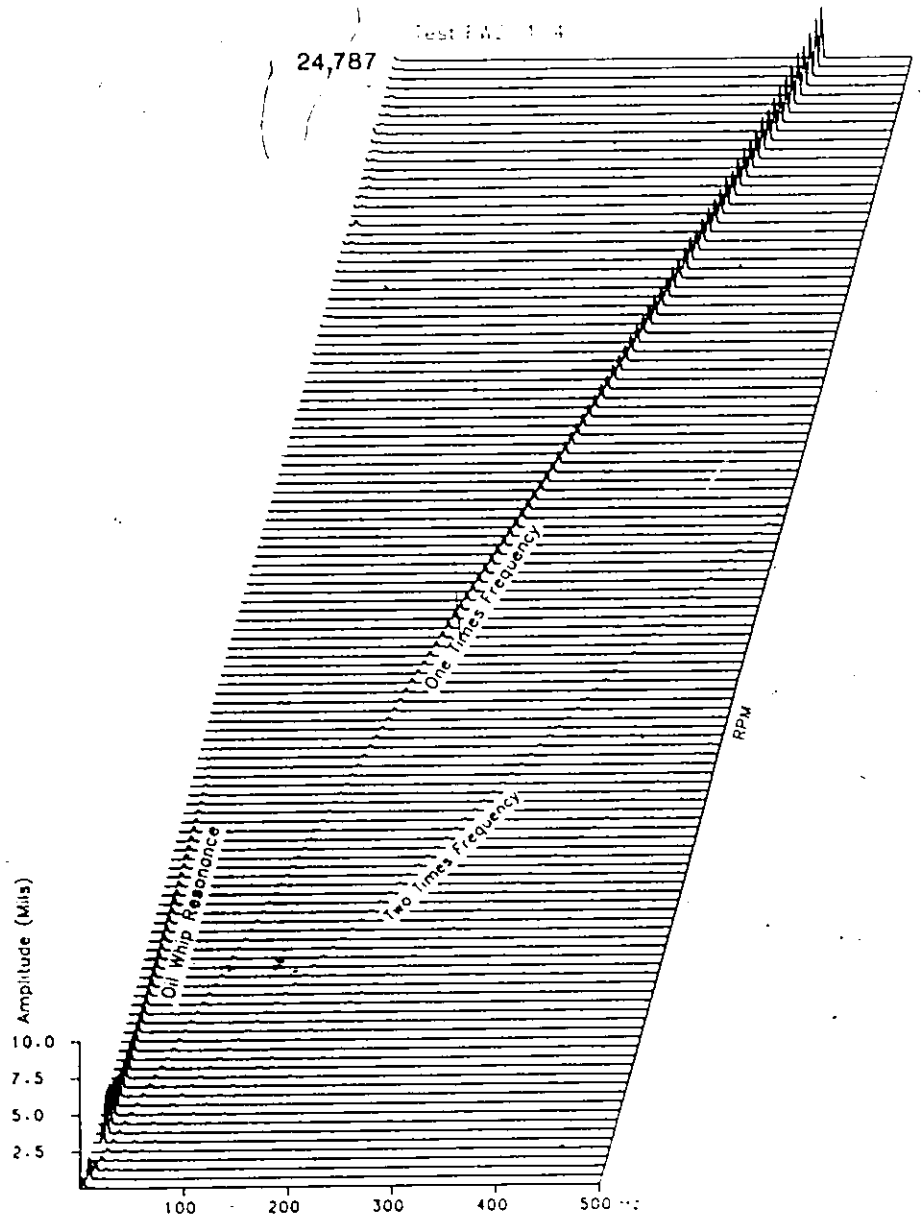

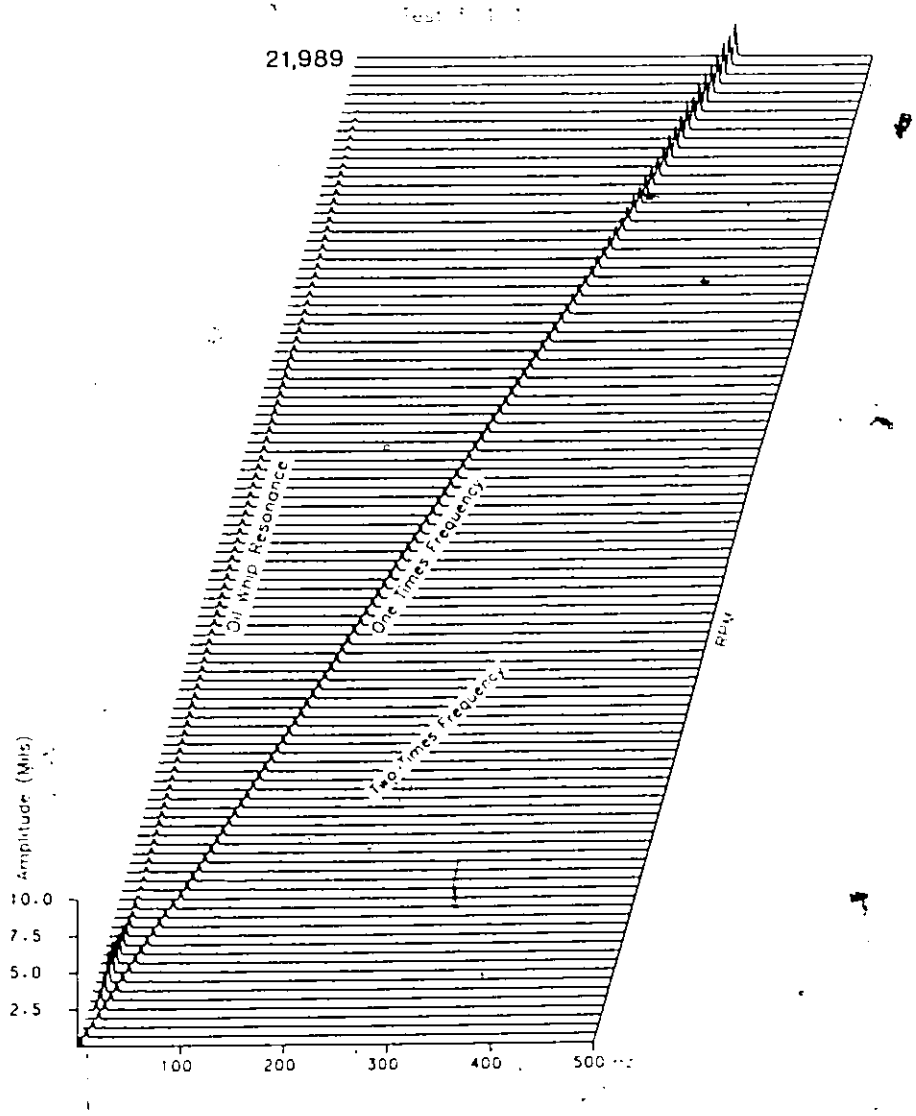

Figure 4.4: Linear Spectral Cascade Plots for FW2 and FW3 Rotors.

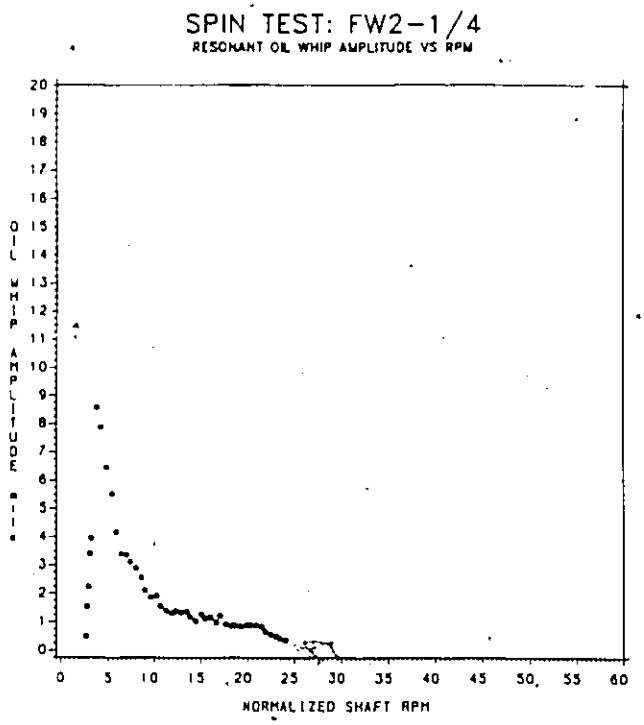

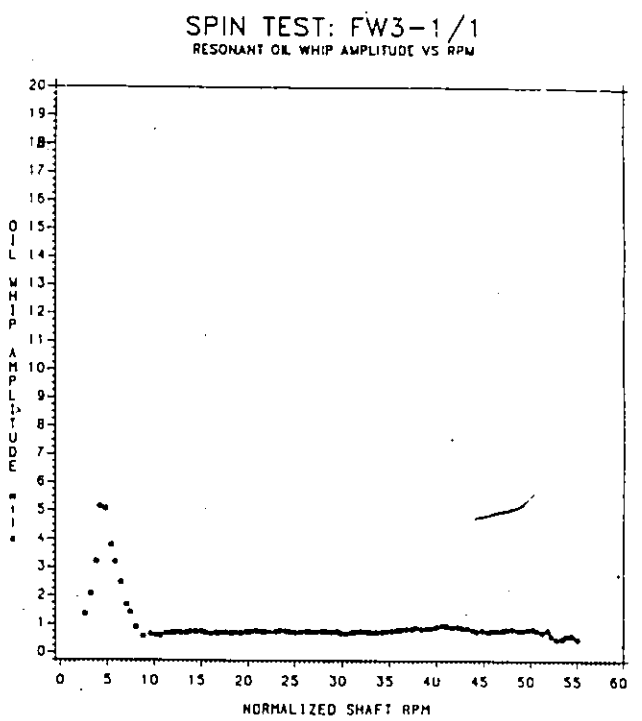

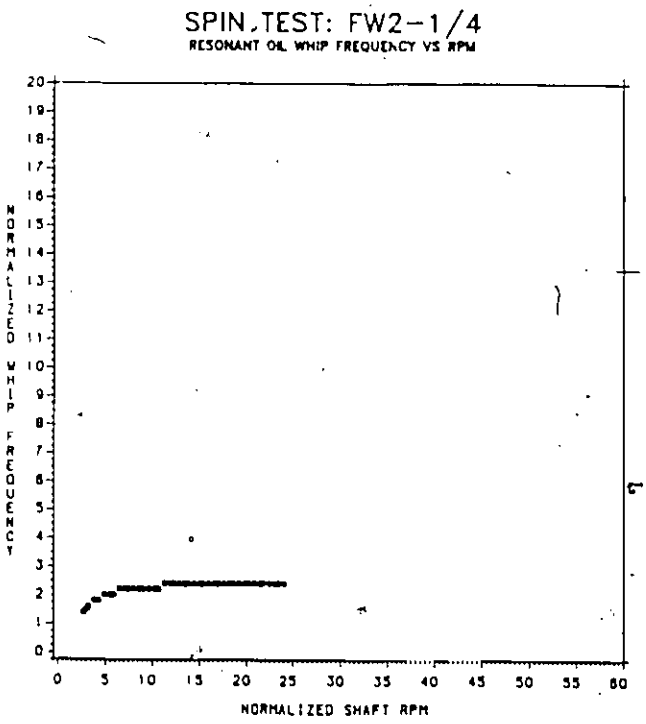

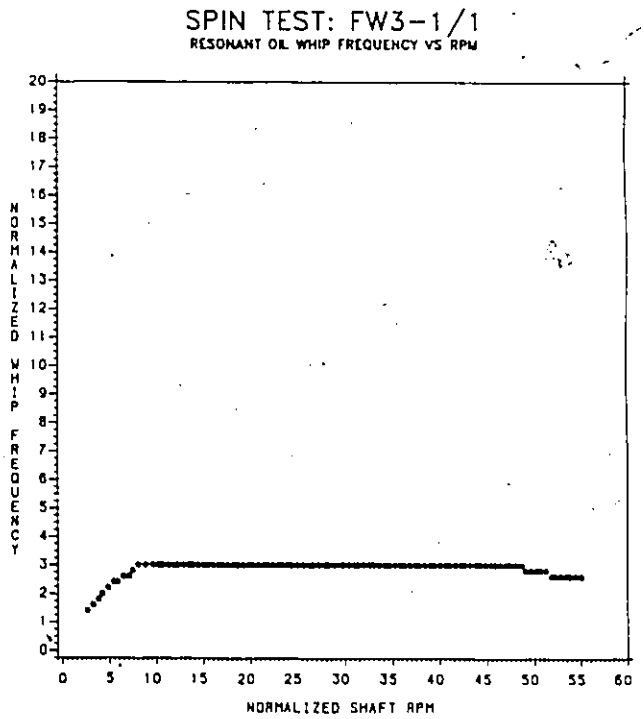

Figure 4.5: Resonant Whip Parameters vs Shaft RPM.

Chapter V
DYNAMIC RESPONSE EXPERIMENTS

A series of state-of-balance vs dynamic response experiments were conducted to record the individual and combined effects of the various parameters involved in rotor balancing. Flywheel FW3A was used for these experiments since this rotor was found to be dynamically well behaved and since its metal hub design allowed for easy alteration of temporary balance weights. The speed range used in these tests was 0-20,000 RPM.

The damper pressure was maintained at its lowest level (5 psi) for the first six experiments, in order to maintain consistent damper characteristics and to minimize oil flow induced resonant whip [43] and high damping induced resonant whip [17]. Experiment FW3A-BD-6 required that the balancing procedure be performed under vacuum because as the rotor balance condition was improving, dynamic instability from windage effects were influencing the rotor response.

5.1 FW3A-BD-1; 'As Is' Response

This first experiment was performed to obtain a record of synchronous dynamic response, without "slow-roll" vector or runout nulling (i.e. the signals as delivered by the monitoring system), of the unbalanced rotor over the test window Figure 5.1. The filtered synchronous amplitude at critical speed was beyond 50 mils for the lower plane. The recorded phases were close to being equal over the whole testing range, indicating a predominant static imbalance. There was no evidence of oil whip resonance occurring due to the high damper

loads from the unbalanced rotor. It should be noted that once the rotor is operating above first critical, it assumes a fixed attitude over the speed range because of the available flexibility of the quill shaft drive.

SPIN TEST: FW3A-BD-1

AMPLITUDE VS RPM (PLANE 1 & 2)

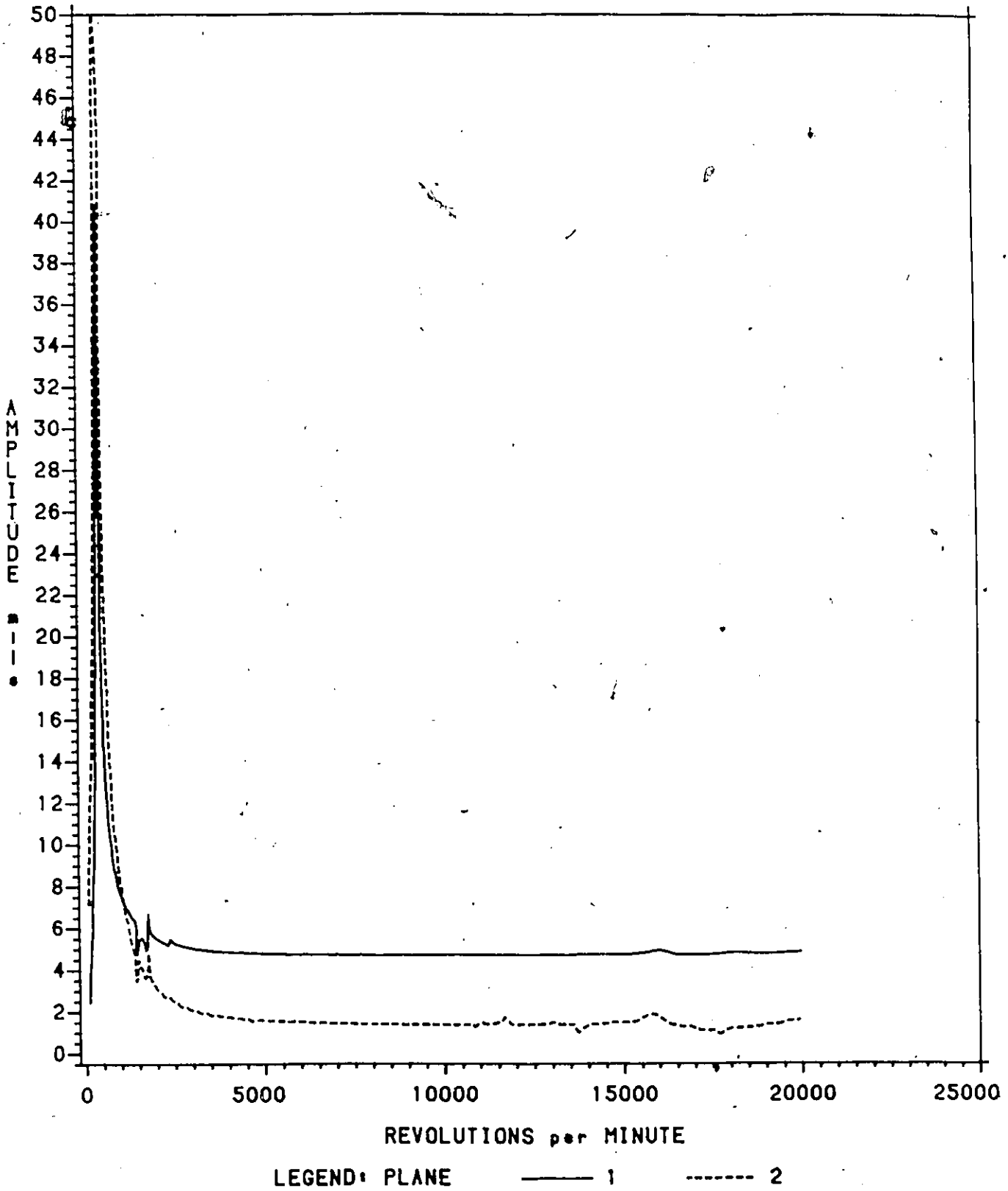

Figure 51: FW3A-BD-1. 'As Is' Rotor Dynamic Response.

5.2. FW3A-BD-2. 'As Is' Response With Nulling

This experiment is of the same nature as the previous one with the slow roll vector being subtracted from the synchronous filtered dynamic response signals through the DVF-2 tracking filter's nulling circuitry. As can be expected, the recorded amplitude Figure 5.2 for the lower plane was again beyond 50 mils going through critical and the phases were close to equal over the whole testing range, indicating a predominant static imbalance. This signal is the true rotor dynamic response and, logically, its general behavior does not change with nulling or removal of runout vector.

What is significant, however, is the above critical motion where rotor state of balance can be observed and where balance data is collected. From rotor to rotor,the runout vector is arbitrary in both magnitude and phase. For this rotor, it is clearly out of phase and of significant magnitude. Without runout consideration, the unbalanced rotor appears to run quite true showing a motion of about 5 mils in plane 1 and 1 mil in plane 2 whereas the true dynamic motion is over 8 mils in plane 1 and just under 12 mils in plane 2. Again, no evidence of oil whip occurred during this experiment.

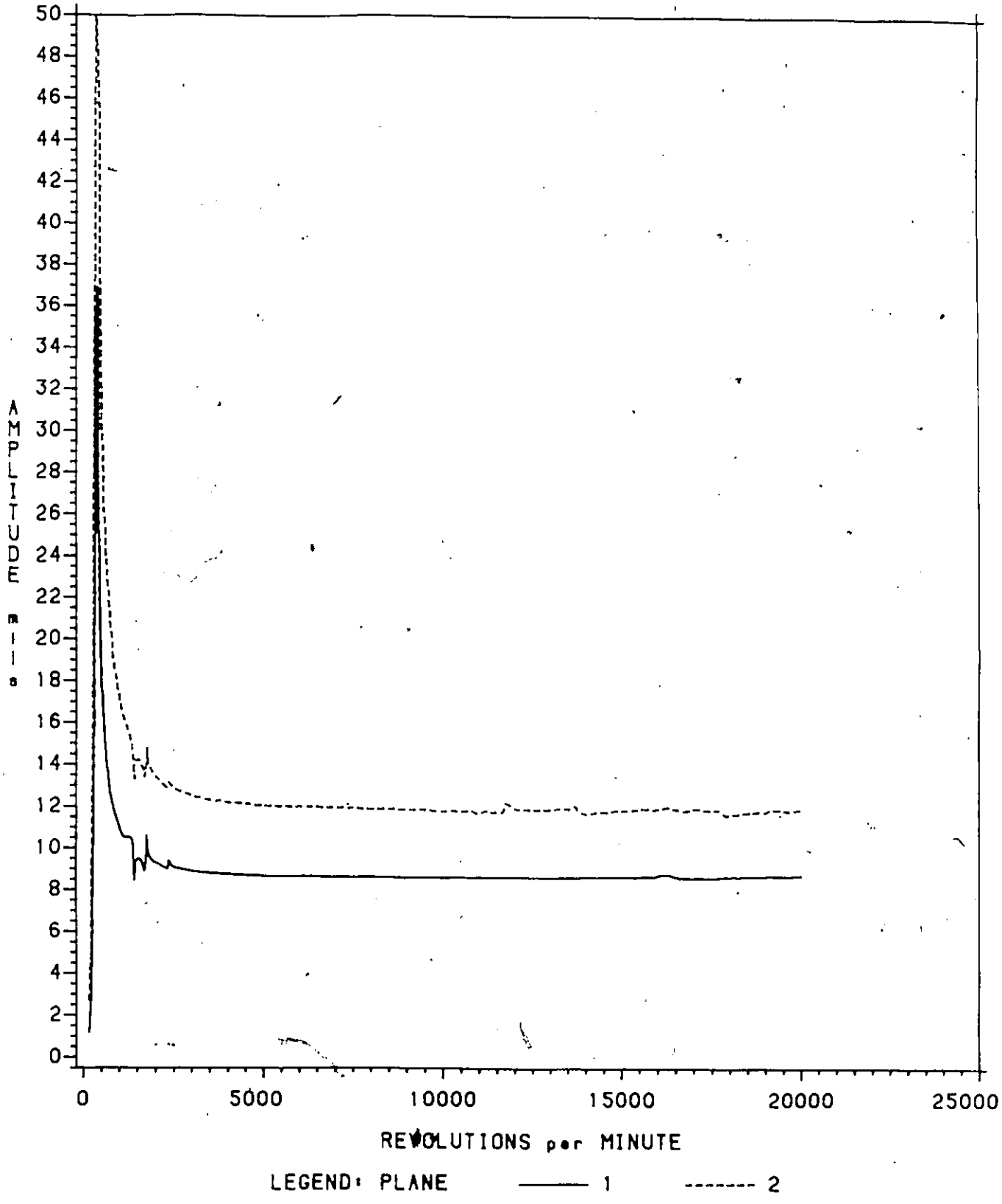

Figure 5.2: FW3A-BD-2. Slow-Roll Effects on 'As Is' Response.

5.3 *FW3A-BD-3; Two-Plane Balance Without Nulling*

The effect of using the two-plane influence coefficient balancing method, without nulling, is shown in this experiment. The synchronous filtered dynamic response shown in Figure 5.3 clearly indicates the procedure to be inadequate. Balancing was done at 1500 RPM and correction weights were determined as:

1. Upper plane 35,99 grams @ 329 degrees.
2. Lower plane 41,96 grams @ 150 degrees.

Comparison of this response should be made with that shown in Figure 5.1 on page 43. The improvement is obvious but clearly the procedure is not adequate.

The rotor dynamic response was unaffected by windage effects throughout the balance procedure. Again, it should be noted that no evidence of oil-whip occurred in this experiment.

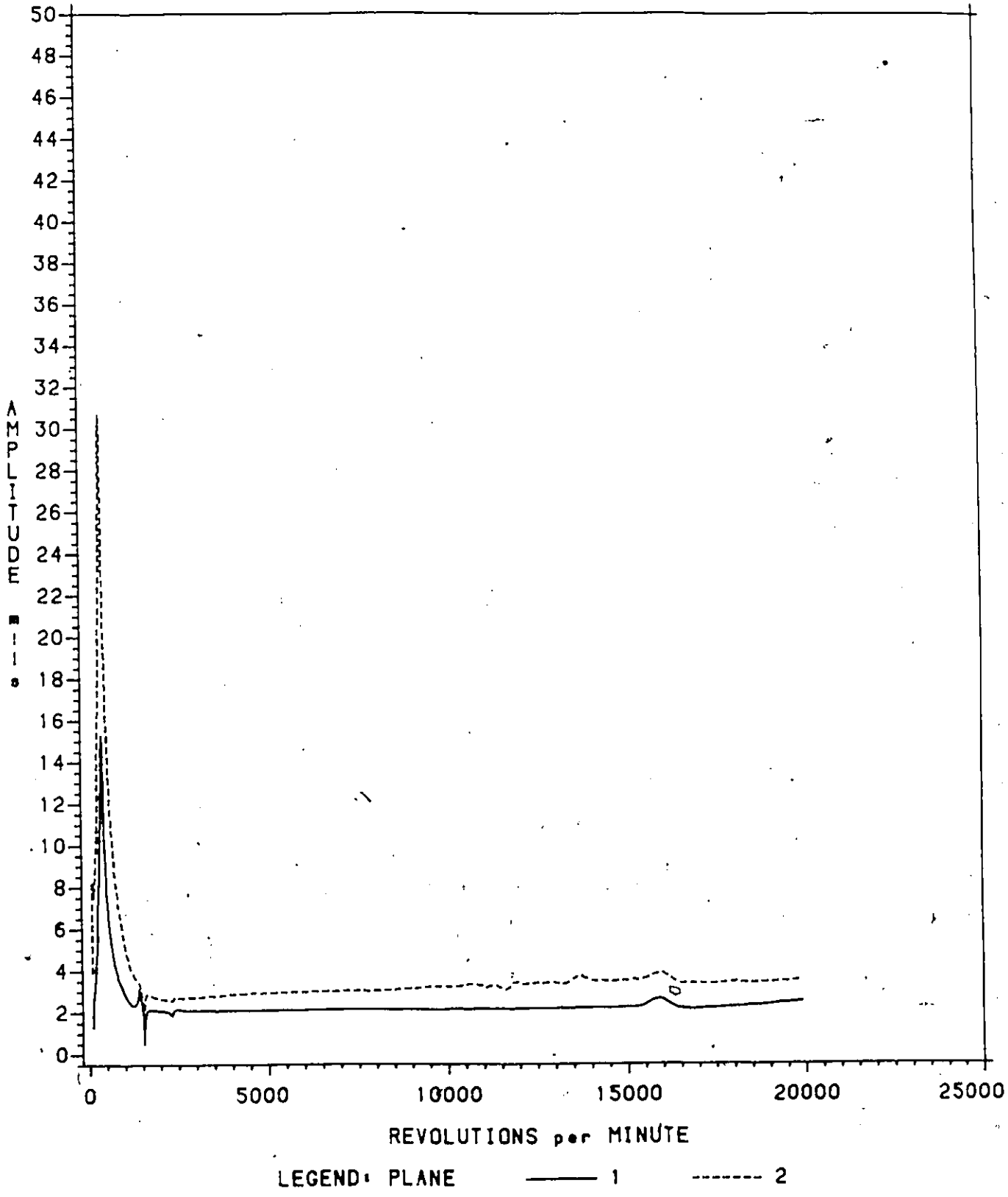

Figure 5.3: FW3A-BD-3. Two-Plane Balance Without Nulling. Effect on Rotor Dynamic Response.

5.4 FW3A-BD-4; Two-Plane Balance With Nulling

This experiment looked into the effects of using two plane balancing with nulled runout signals. Thus, true rotor dynamic response is being monitored and a marked improvement is apparent. Here, Figure 5.4, should be compared with Figure 5.2 on page 45. Amplitudes through critical speed are significantly improved and dynamic response above critical averages about one mil. At the balance speed of 1500 RPM, the correction weights were determined to be:

1. Upper plane 42,82 grams @ 175 degrees.
2. Lower plane 25,49 grams @ 19 degrees.

It is interesting to note that the upper plane correction weight, which was much larger than the lower plane correction weight, was close to the region where the large static imbalance was finally found to be located in experiment FW3A-BD-6.

The most significant result, however, is that for the first time, the rotor induced dynamic behavior is beginning to show. As stated, this is seen to be a key evaluation requirement for composite material rotor assessment. Here, some center-of-mass shifting is suggested by the increasing rotor speed or with increasing rotor radial dilation. Again, no resonant oil whip appeared in this experiment, and the dynamic response was unaffected by windage effects throughout the balance procedure.

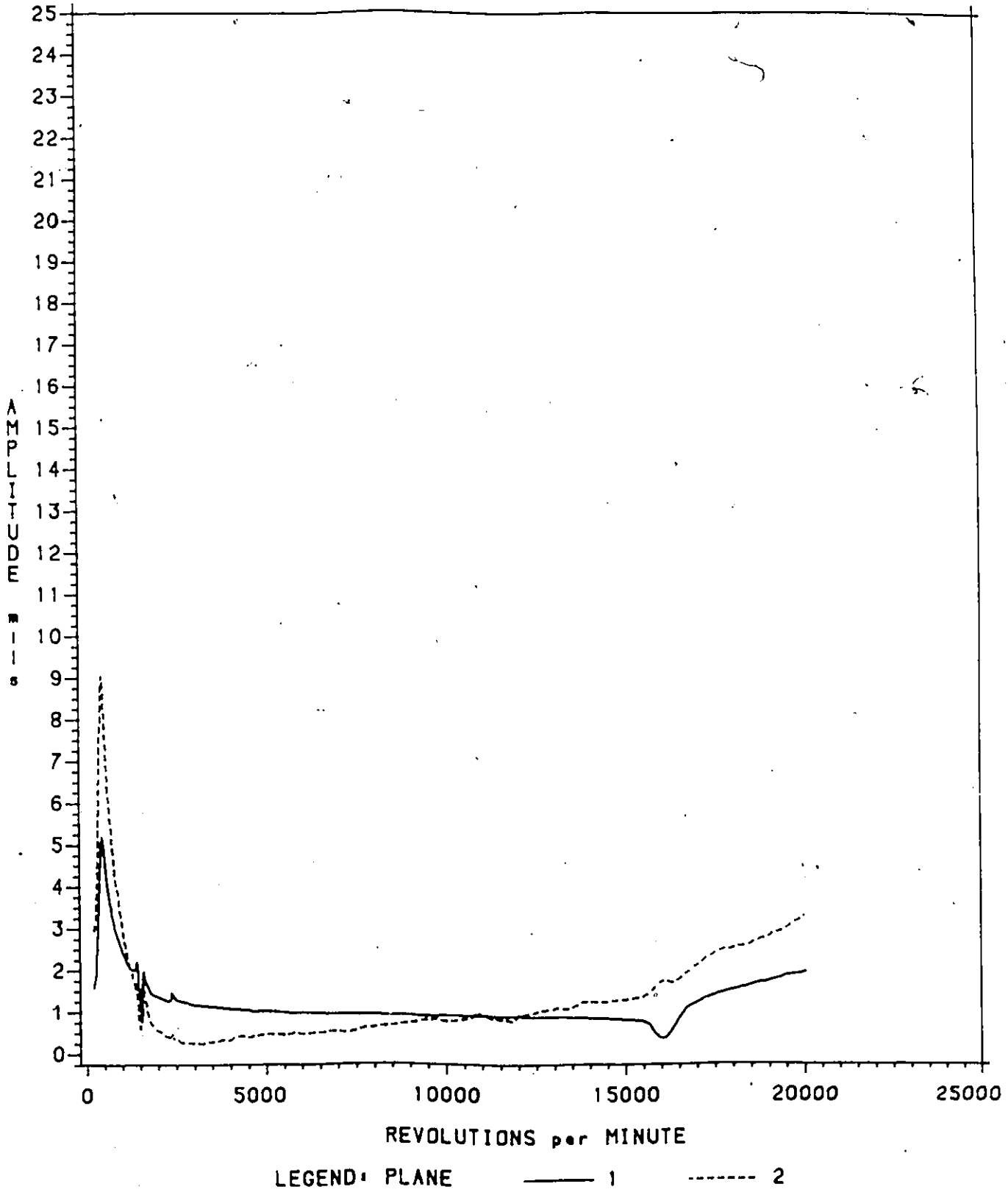

Figure 5.4: FW3A-BD-4. Two-Plane Balance With Nulling. Effect on Rotor Dynamic Response.

5.5 FW3A-BD-5; Static/Couple Balance Without Nulling

Experiment FW3A-BD-5's purpose was to observe and record the dynamic response of a rotor which had its static and dynamic imbalances balanced independently but without nulling. The synchronous filtered dynamic response Figure 5.5 displays similar characteristics to those found in [51], where the researchers investigated the effects of out of roundness, as part of their "Experimental Evaluation of the Exact Point-Speed and Least-Squares Procedures for Flexible Rotor Balancing by the Influence Coefficient Method". The results show a bottoming out of the measured vibration amplitude(s) at balance speed only (1500 RPM) but clearly an acceptable state-of-balance has not been achieved and rotor induced dynamic behavior cannot be evaluated.

The correction weights were;

1. Static correction weight of 7,23 grams @ 58 degrees.
2. Dynamic correction weight of 40,84 grams @ 320,1 degrees, upper plane.
3. Dynamic correction weight of 37,41 grams @ 142 degrees, lower plane.

Again no resonant oil whip was observed and the rotor dynamic response was unaffected by windage effects throughout the balance procedure.

SPIN TEST: FW3A–BD–5

AMPLITUDE VS RPM (PLANE 1 & 2)

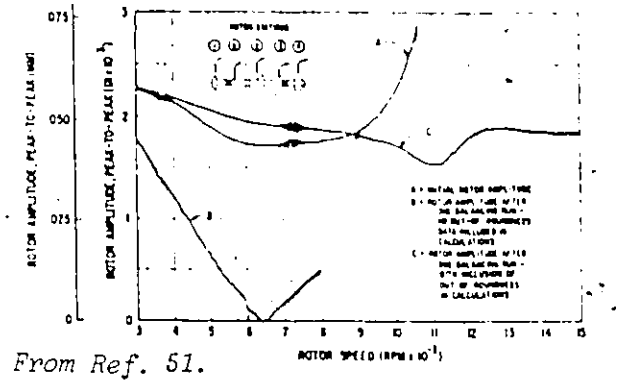

From Ref. 51.

Fig. 14 Vertical rotor amplitudes at station 1—initial condition of two-mass rotor (conical unbalance) and after one balancing run, with and without inclusion of shaft out-of-roundness data in the correction weight calculations

Figure 5.5: FW3A–BD–5. Static/Couple Balance Without Nulling. Effect on Rotor Dynamic Response.

5.6 FW3A-BD-6; Static/Couple Balance With Nulling

This test is a repeat of FW3A-BD-5 with the slow roll runout vector incorporated throughout the experiment via the DVF-2 tracking filter's nulling circuitry. The outstanding differences from FW3A-BD-5 are the relative sizes of the correction weights, their location and also the dynamic response, shown in Figure 5.6. Here, rotor amplitudes through critical speed are exceptionally low and the above critical speed dynamic response is near zero (approximately 0.1 and 0.3 mil in the upper and lower planes respectively). It is clear that this procedure provides a precision state-of-balance thus allowing accurate evaluation of rotor induced dynamic behavior. For this rotor, there is a growth in amplitude above 15000 RPM. This behavior, where the rotor center of mass changes with speed for composite flywheels was also observed by R.S. Steele [46]. The phase angles in each plane were very close during the amplitude growth which occurred at speeds beyond 15000 RPM, indicating an increase in the state of static imbalance. Because the rotor in the previous experiments had gross imbalances due to inappropriate correction weights, the slight change in balance condition occurring from dynamic loading would have been insufficient to alter the response. Only in experiment FW3A-BD-4 was this growth phenomenon slightly present.

Another interesting observation was that after performing the static correction on FW3A-BD-6, the rotor showed instabilities while rotating at balance speed (1500 RPM) under atmospheric pressure. None of the previous balancing experiments showed this phenomena. As such the procedure had to be performed under vacuum, from runout nulling through the trial weight runs, in order to avoid windage effects on the spinning rotor.

The correction weights were;

1. Static correction weight of 20,71 grams @ 140,7 degrees

2. Dynamic correction weight of 17,99 grams @ 141,6 degrees, upper plane.

3. Dynamic correction weight of 17,41 grams @ 322,6 degrees, lower plane.

The primary imbalance was the static component. The highest occurrence of resonant oil whip occurred during this last experiment due to the high state-of-balance in the rotor and the resulting low journal bearing loads in the damper assembly as discussed in the previous chapter.

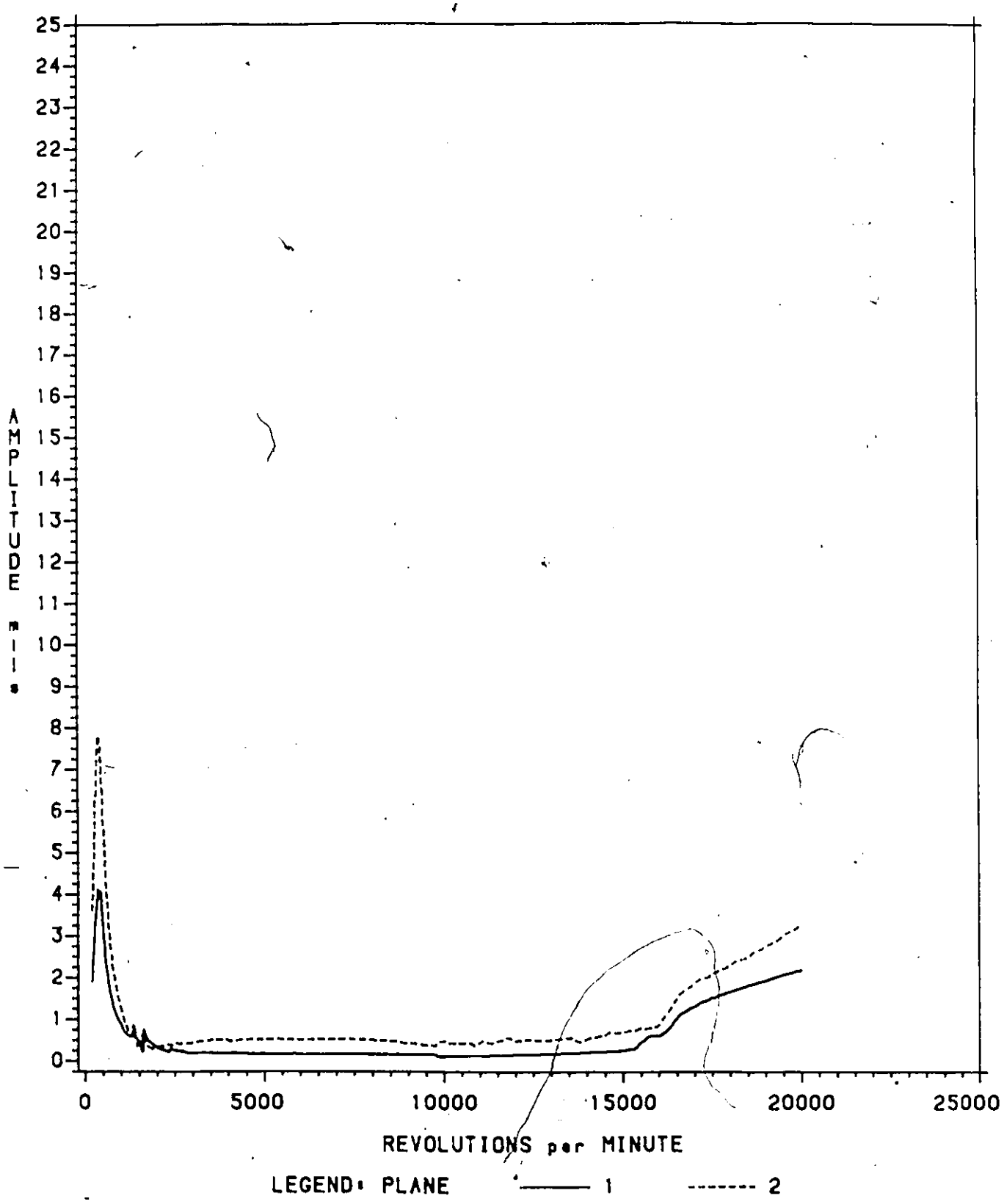

Figure 5.6: FW3A-BD-6. Static/Couple Balance With Nulling. Effect Rotor Dynamic Response.

5.7 *FW3A-BD-7; Moment Induced Retrograde Whirl*

This investigation was done to observe the effects of a pure couple imbalance acting upon a flexibly/pendulously mounted rotor. While this was academically motivated, it could also prove to be important for the upcoming tests where behavior evaluations of the four rotors were to be made. Rotor FW3A was found to slowly precess in a retrograde fashion, the precessional frequency being inversely proportional to the flywheel spin frequency, as shown in Figure 5.7. This behavior corresponds to the special case in classical gyrodynamics theory of a spinning top precessing without nutating under the effects of a gravity moment [29,30,53]. The moment, in this case, would be applied in the opposite direction so as to induce a retrograde rather than forward precession.

As well, the experimental data correlates with the first or lowest retrograde whirl branch of Den Hartog's classical model of a disk mounted at the end of a rotating cantilever[16]. This correlation was done using Thomson's [52] upgraded version of the model to include effects stiff sections of shaft.

The static imbalance was removed using the static/couple derivation with nulled vibration signals approach, leaving the rotor with a couple imbalance, which was then evaluated. From that point on, the couple imbalance could be adjusted to prescribed values for experimental analysis. Only one complete set of repeatable data was gathered for Figure 5.7, with a moment imbalance of 3249 g–cm**2. Other attempts with higher and lower amounts of couple imbalances induced retrograde precessions; but no complete correlation was drawn as the rotor amplitude either tended to "jump" [15][50], or simply die out because of the profound effects of damping on retrograde whirls [4,16,52].

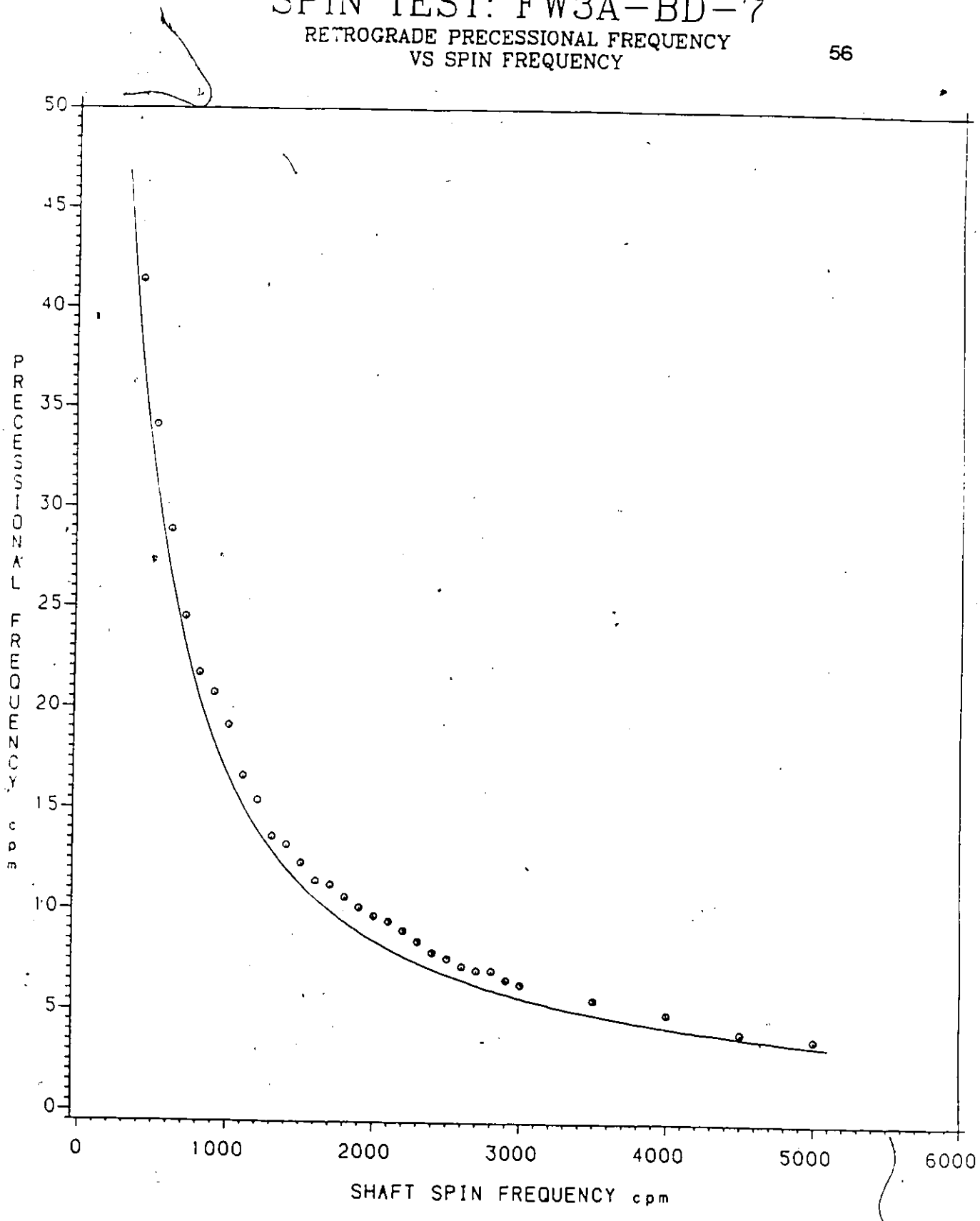

Figure 5.7: FW3A-BD-7. Moment Induced Retrograde Whirl Retrograde Whirl Frequency vs. Rotor Spin Frequency.

The dynamics involved can be broken down into the following major rigid body components. As the flywheel rotated about its center of gravity (C.G.) which was along its center of geometry, from static balancing, the couple imbalance, represented by the point masses "m" in Figure 5.8, tended to tilt the rotor which in turn introduced a counteracting moment from gyrodynamic disk effects [16] and also from the bent spindle shaft as shown in Figure 5.8. As the rotor angular velocity increased, it assumed a constant tilt configuration, as was observed in previous experiments as well, independent of the shaft spin velocity, leaving the rotor with a net, constant, external moment being applied by the slightly bent spindle. Under the dynamic conditions stated above, retrograde precession will occur whenever the amount of damping allows.

Another case of retrograde precession was observed at the University of Ottawa facility. Upon test number 5 of rotor CH-19, a low frequency retrograde precession (0.083 Hz.) set in after 30 seconds, while coasting at 20,000 RPM. The test was prolonged until the amplitude grew almost exponentially (jump phenomenon [15,11]), limited only by the upper catcher restraint, destroying the upper set of proximity probes. The retrograde frequency was observed to increase as CH-19's rotational speed decreased during braking.

CH-19 was a one inch thick, nineteen inch diameter S2L material disk supported by a flex-ring attachment, as was shown in Figure 4.2 on page 35. The rotor was statically balanced using the filtered upper plane vibration readings. However, at this point in the program, nulling was not being used and further, dynamic balancing was not considered because of the disk thickness which limited the effectiveness of plane separation. It is very likely that the retrograde precession was moment induced and could have been eliminated or curbed if the damper pressure had been increased from its 15 psi setting.

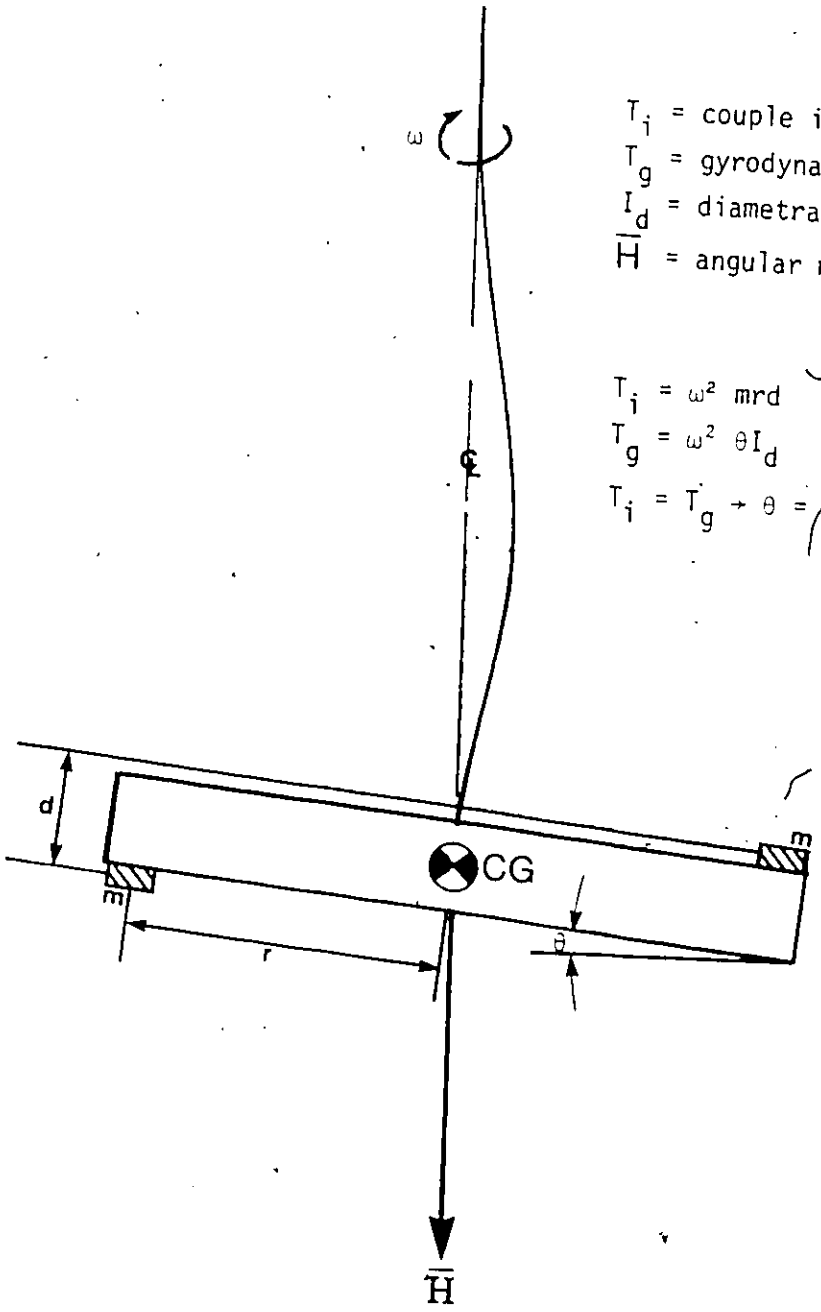

T_i = couple imbalance induced torque
T_g = gyrodynamic induced torque
I_d = diametral moment of inertia
$\bar{H}$ = angular momentum

$T_i = \omega^2 \, mrd$
$T_g = \omega^2 \, \theta I_d$
$T_i = T_g \rightarrow \theta = \frac{mrd}{I_d}$ independent of ω

Figure 5.8: Effects of Couple Imbalance.

In reference [31] A. Keith Miller made the following observation while spin testing a 24 spoke Sandia "wagon wheel" flywheel. A very low frequency (approximately 3 Hz) retrograde whirl motion developed as the twenty-four spoked flywheel drifted down in speed from 20,000 RPM. The amplitude of this whirl increased approximately exponentially with time until the motion became so violent that the test had to be stopped. Several attempts were made to allow the flywheel to drift down in speed, all resulting in the development of the same, nearly classical, instability.

Investigation into the possible cause of the low frequency retrograde whirl of the flywheels during this first series of tests revealed that the oil pressure in the squeeze-film damper assembly was below normally prescribed conditions. An obstruction in the hose which supplies the feed oil to the damper assembly was removed, the oil pressure was increased, and a second series of tests using only the twenty-four spoked flywheel was performed.

The instability as the flywheel drifted down in speed from 20,000 RPM was no longer observed.

Our experiences show a definite curbing effect from damping as well as a definite link between couple imbalance and retrograde precession. We do not believe the damper to be the cause of retrograde instability but rather a controlling factor.

Chapter VI
ROTOR BALANCING AND EVALUATION

Four high energy density fibre composite rotors were built and three were tested. Table 1 and Table 2 list the rotor parameters while the following summarizes their construction.

Flywheel one (FW1) consist of a sheet molding compound (SMC) fibre composite central hub thermally-interference fit to a wet-filament-wound E/XAS carbon outer ring, with an aluminum (7075-T651) flex-ring - steel (SAE 4340) arbour bolting shaft attachment system, fixed onto the SMC hub. The assembled rotor is shown in Figure 6.1.

Flywheel two (FW2) consist of an S2-glass laminated (S2L) fibre composite central hub thermally-interference fit to a wet-filament-wound E/XAS carbon outer ring with a maraging steel (MA-C300) flex-ring - steel (SAE 4340) arbour bolting shaft attachment system, fixed onto the S2L hub. The assembled rotor is shown in Figure 6.2.

Flywheel three (FW3) has a manufactured metallic hub (7075-T651) designed for radial compatibility with a composite ring assembly. The ring assembly consist of an inner wet-filament-wound S2-glass ring and a wet-filament-wound E/XAS carbon outer ring. Each of the components mentioned above were thermally-interference fit. The assembled rotor is shown in Figure 6.3.

Flywheel four (FW4) has a manufactured metallic hub designed for radial compatibility with a composite ring assembly of the same nature as FW3. The hub consist of a thermally-interference fit aluminum (7075-T651) ring insert and

oppositely mounted maraging steel (MA–C300) spoked spring plates held through a central steel (SAE 4340) arbour assembly. The assembled rotor is shown in Figure 6.4.

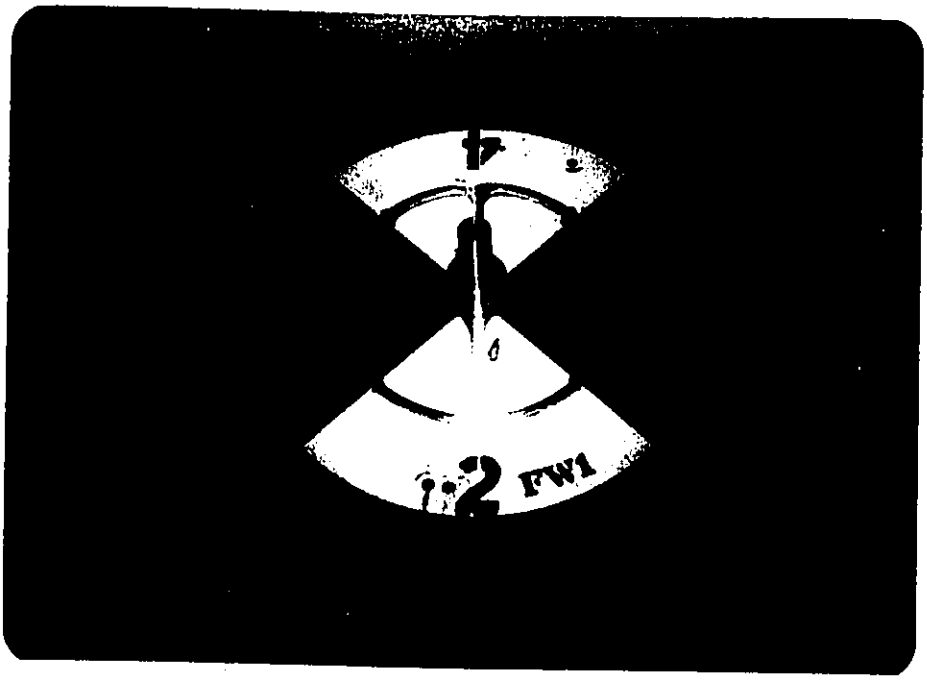

Figure 6.1: Flywheel One (FW1) Assembly.

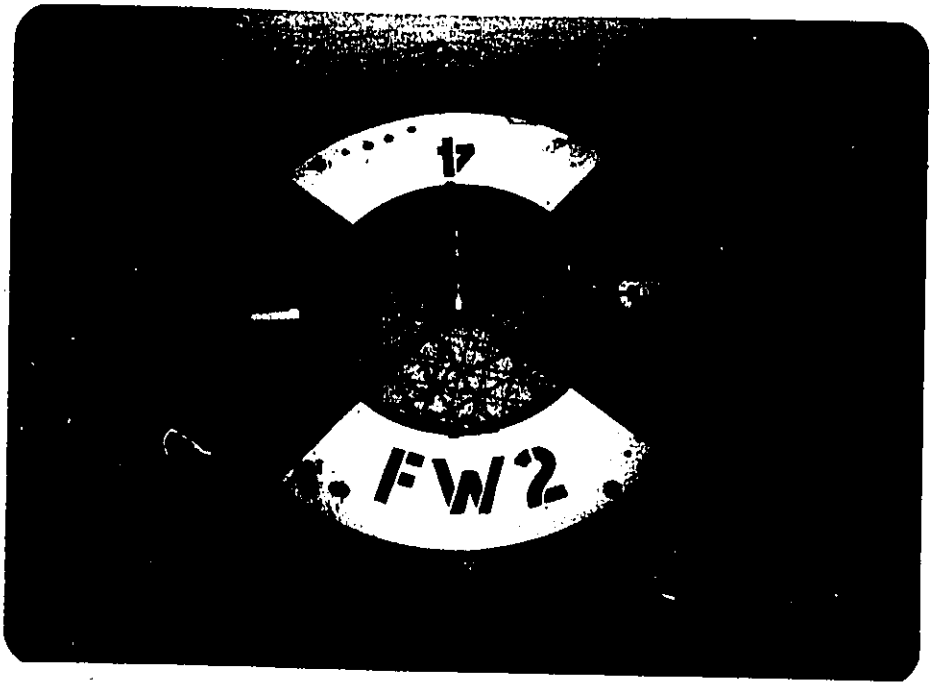

Figure 6.2: Flywheel Two (FW2) Assembly.

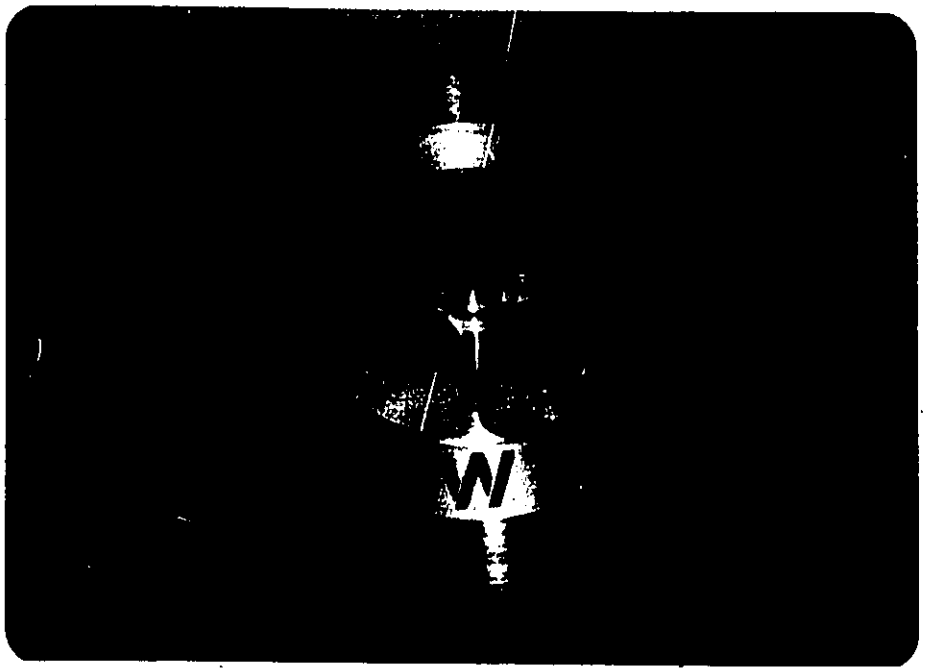

Figure 6.3: Flywheel Three (FW3) Assembly.

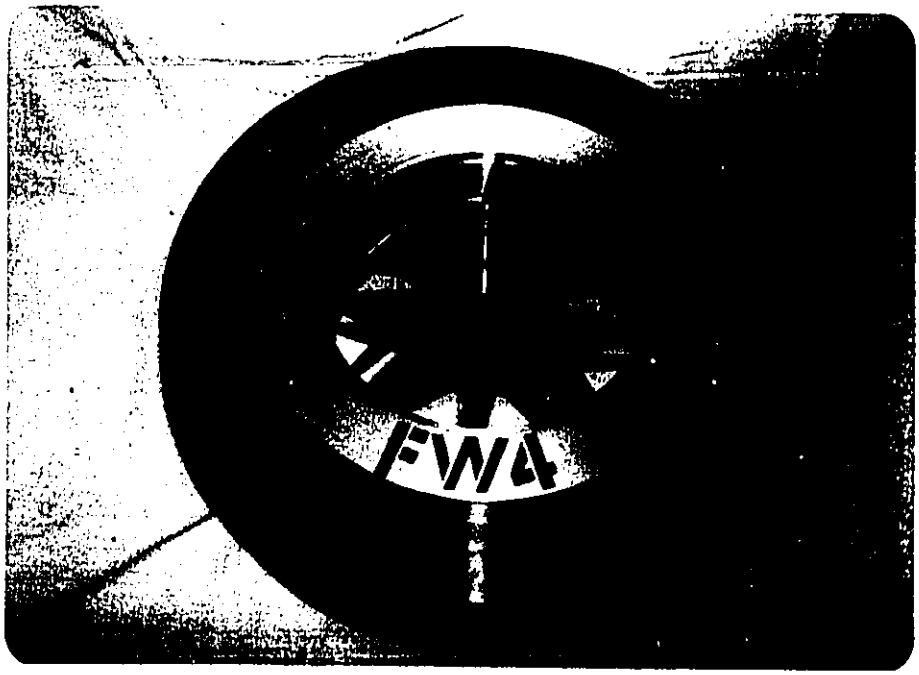

Figure 6.4: Flywheel Four (FW4) Assembly.

Table 1

Composite-Hub Rotors: Design Specification.

ITEM	FW1	FW2
A: ROTOR CONSTRUCTION		
Hub Material	SMC (R65-S2)	S2-G Laminate
Ring Material	E/XAS-Carbon	E/XAS-Carbon
Assembled Hub O.D.; in. (cm)	16.80, (42.67)	18.84, (47.85)
Hub/Ring Int. Pres.; KSI,(MPa)	3.0, (20.7)	3.0, (20.7)
Hub/Ring Assembly	Thermal Fit	Thermal Fit
Bolted Shaft Attachment	FRA System	FRA System
FRA Material	7075-T651 Alu.	C300 Mar. Steel
FRA Bolt Dia.; in. (cm)	10.332, (26.243)	10.550, (26.797)
B: DESIGN PARAMETERS		
Outside Diameter; in. (cm)	24.00, (60.96)	24.00, (60.96)
Axial Thickness; in. (cm)	3.25, (8.25)	2.50, (6.35)
Weight; lbs., (kg)	87.6, (39.7)	70.4, (31.9)
Swept Volume; in^3. (cm^3)	1470, (24079)	1131, (18533)
Design Speed, RPM	18,860	24,760
Stored Energy, KW-Hr	1.00	1.33
En. Density: Wh/lb. (Wh/kg)	11.4, (25.2)	18.9, (41.8)
Cycle Life: cycles	10^5	10^5
Operating Temperatures	-40 to 100°C	-40 to 100°C
C: ULTIMATE PERFORMANCE*		
Ultimate Speed, RPM	25,770	33,520
Failure Mode	Hub Burst	Ring Failure
Energy Stored; KW-Hr	1.87	2.45
En. Density; Wh/lb. (Wh/kg)	21.3, (47.1)	34.8, (76.8)

* It could be noted that the rotors are optimized for a life of 10^5 cycles, not for an ultimate speed test.

Table 2

Metallic-Hub Rotors: Design Specification.

ROTOR CONSTRUCTION	FW3	FW4
Ring Design	Design No. 1 or 2	Design No. 1 or 2
Hub Design	Flex-Rim (FRH)	Spring-Spoke (SSH)
Hub Material	7075-T651 Alu.	7075-T651 Alu. ring liner with C300 Mar. Steel Spoke Plates
Hub/Ring Assembly	Thermal Fit	Thermal Fit
Ring Radial Compatibility	Rim Flexing	Spoke Flexing

RING DESIGN	DESIGN NO. 1	DESIGN NO. 2
A. DESIGN PARAMETERS		
Ring Construction	Bianhular: S2-Glass Inner, E/XAS Outer	Biannular: S2-Glass Inner, E/XAS Outer
Outside Diameter: in. (cm)	24.00, (60.96)	24.00, (60.96)
Interface Diameter: in. (cm)	17.246, (43.805)	18.040, (45.822)
Inside Diameter: in. (cm)	12.650, (32.131)	12.644, (32.116)
Ring/Ring Int. Pres: KSI, (MPa)	2.00, (13.8)	2.25, (15.5)
Ring Assembly	Thermal Fit	Thermal Fit
Axial Thickness: in. (cm)	3.45, (8.76)	3.45, (8.76)
Weight: lbs. (kg)	78.0, (35.4)	78.7, (35.7)
Swept Volume: in^3. (cm^3)	1561, (25,567)	1561, (25,567)
Design Speed: RPM	21,900	21,775
Stored Energy: KW-Hr.	1.33	1.33
En. Density: Wh/lb. (Wh/kg)	17.1, (37.7)	17.0 (37.4)
Cycle Life: cycles	10^5	10^5
Operating Temperature	-40 to 100°C	-40 to 100°C
B: ULTIMATE PERFORMANCE*		
Ultimate Speed: RPM	29,200	32,250
Failure Mode	E/XAS Ring	E/XAS Ring
Energy Stored: KW-Hr	2.37	2.93
En. Density: Wh/lb. (Wh/kg)	30.4, (67.0)	37.2, (82.1)

* It could be noted that the rotors are optimized for a life of 10^5 cycles, not for an ultimate speed test.

6.1 Composite Hub Rotors

For the composite hub flywheels, it was proposed that the static imbalance of the principle components, namely the SMC and the S2L hubs and corresponding E/XAS–Carbon fibre rings, be determined prior to their assembly. This would have allowed for minimal corrective measures to be brought to the assemblies by opposing the rotor components' heavy sides during the assembly procedure. Eventually it was determined that the carbon rings had very little inherent static imbalance as did the S2L material, while the SMC hub possessed a significant amount of static imbalance.

6.1.1 Carbon Ring Static Imbalance

After machining and grinding of the outside diameter of the E/XAS–Carbon rings, Figure 6.5, they were placed on previously balanced winding mandrels, secured and positioned by shrinking the steel mandrel with liquid nitrogen and inserting the proper amount of weighed shim stock in between the mandrel and ring to obtain a snug fit, Figure 6.6.

The temporary assemblies were then set on a horizontal shaft static balance rig as shown in Figure 6.7. No measurable amounts of static imbalance were found for the rings manufactured. The static balance rig's sensitivity was measured at around 5,7 g–cm or 0,08 oz–in.

[2] Both the SMC and S2L hubs were supplied by Owens–Corning, Granville, Ohio.

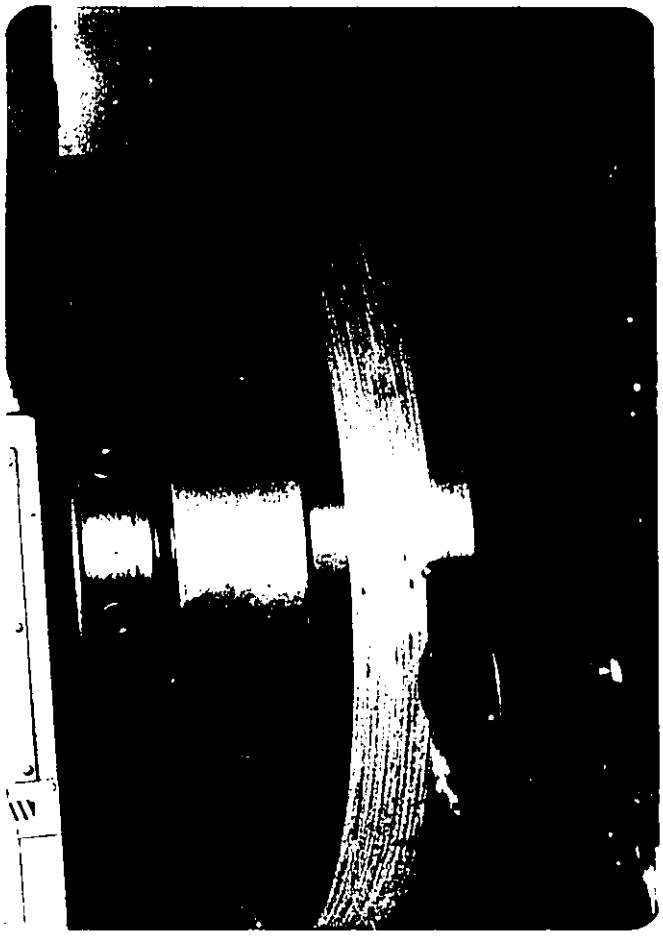

Figure 6.5: Grinding E/XAS–Carbon Fibre Ring Outside Diameter.

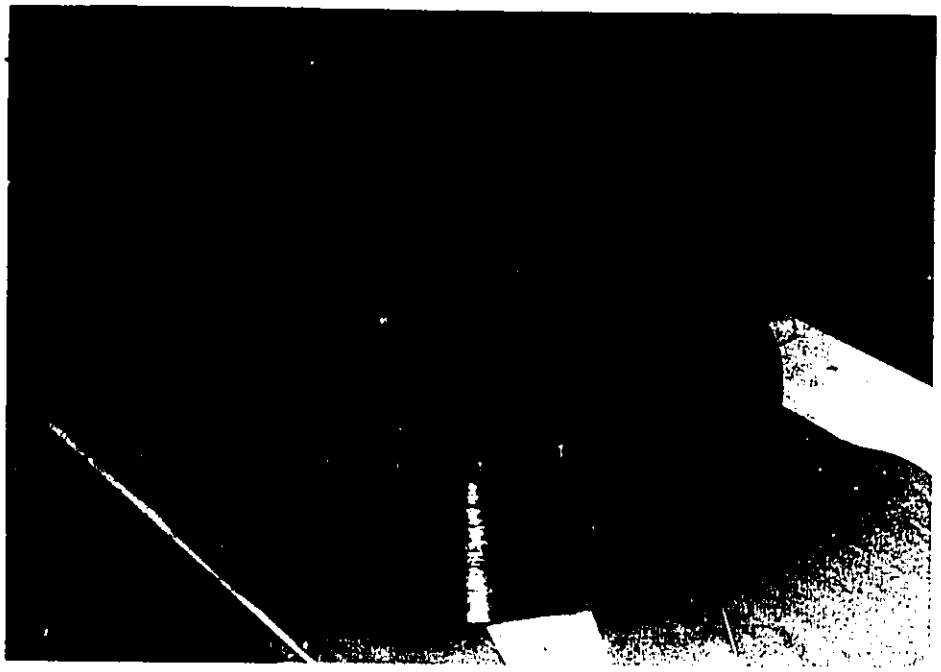

Figure 6.6: Central Mandrel Cooldown Using Liquid Nitrogen.

Figure 6.7: E/XAS Carbon Ring Static Imbalance Verification.

6.1.2 Hub Balance Corrections

The composite hubs' state of static balance were measured in the horizontal setup, as used for the E/XAS–Carbon rings, and cross verified in the dynamic balance rig. By temporarily attaching flex–rings (top and bottom) with upper arbours to the composite hubs, the temporary assemblies could then be set in the horizontal balance rig, as shown in Figure 6.8. To confirm the location and the amount of imbalance, the assemblies were then mounted in the dynamic balance rig which was developed by the author [28] as shown in Figure 6.9. Only the upper plane data was used at the time. The results correlated and because the carbon rings did not possess any appreciable amount of imbalance, the hubs were balanced by drilling out material from the mid section of the disk, no deeper than one inch. Figure 6.10 shows the SMC hub being drilled on the heavy side and Figure 6.11 is a view of the SMC hub prior to being inserted in the E/XAS Carbon ring after cooling down both components to Liquid Nitrogen temperature. The static balance correction is quite visible on the SMC hub.

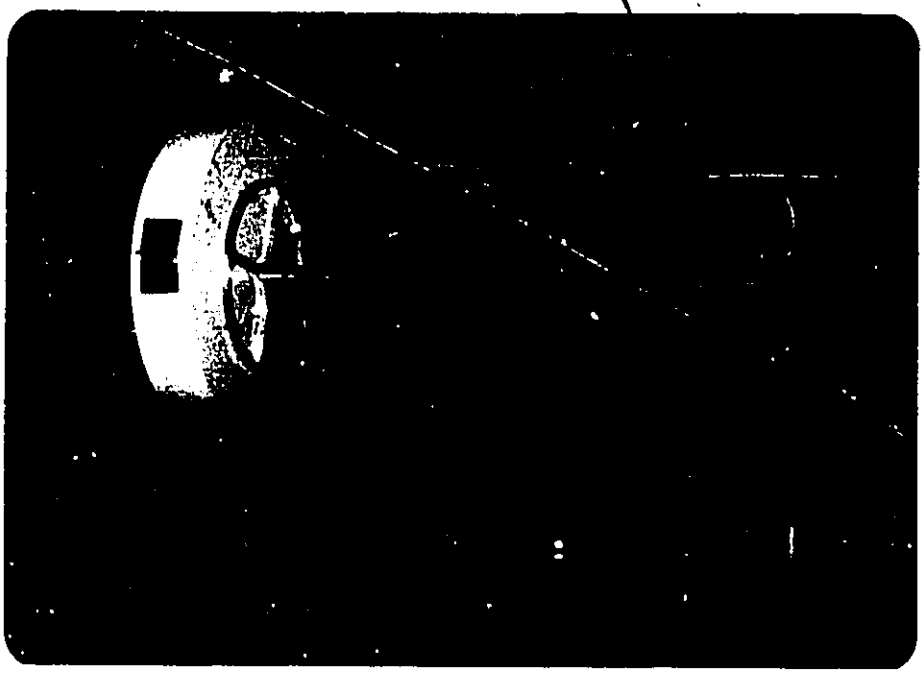

Figure 6.8: SMC Hub Static Balance Procedure.

Figure 6.9: Dynamic Balance Rig. The Dynamic Balance Rig Seen Door Open and with the Two Plane Practice Rotor Installed.

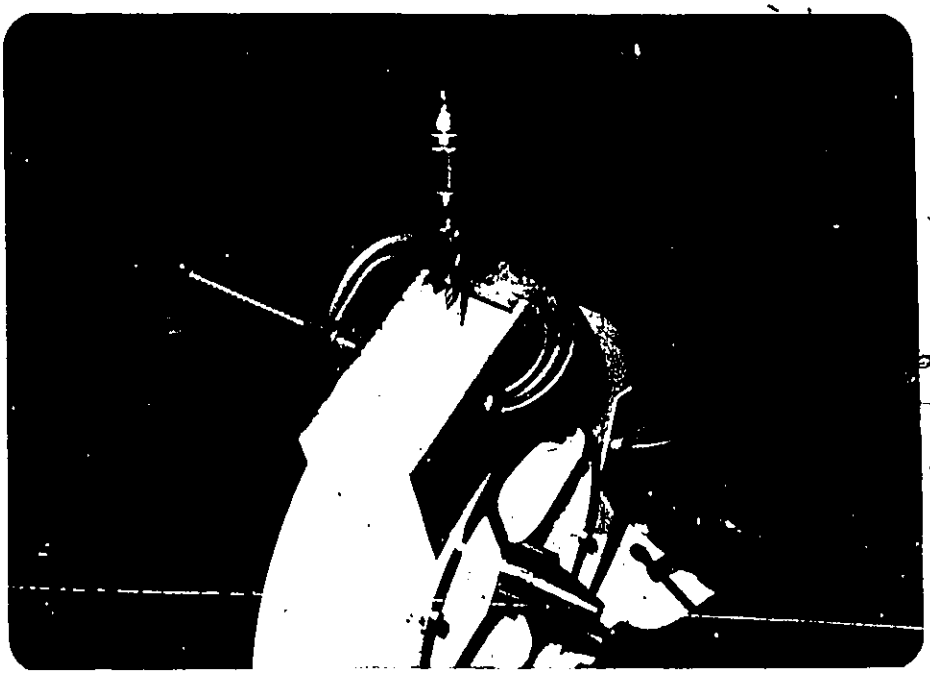

Figure 6.10: Mass Removal on SMC Hub, Static Balancing.

The S2L material used for FW2 had one of its surfaces slanted because of a malfunction occurring during the heat and pressure curing stages of manufacturing. This was the source of machining error which introduced an apparent imbalance in the hub. Although the level surface was identified and marked as "TOP", to avoid introducing tilt on the upper arbour, during the process of drilling the four holes for the flex ring attachment studs, the hub was set on each face to facilitate drilling from both surfaces. When the hub was resting on the tapered face, the holes drilled were thrown off slightly and gave rise to an apparent imbalance.

It was later found that the S2L hub was not so much out of balance but not before having removed material from the hub in the same manner as the SMC hub. Figure 6.12 testifies to the amount of apparent imbalance which was determined and shows the components just prior to their final assembly.

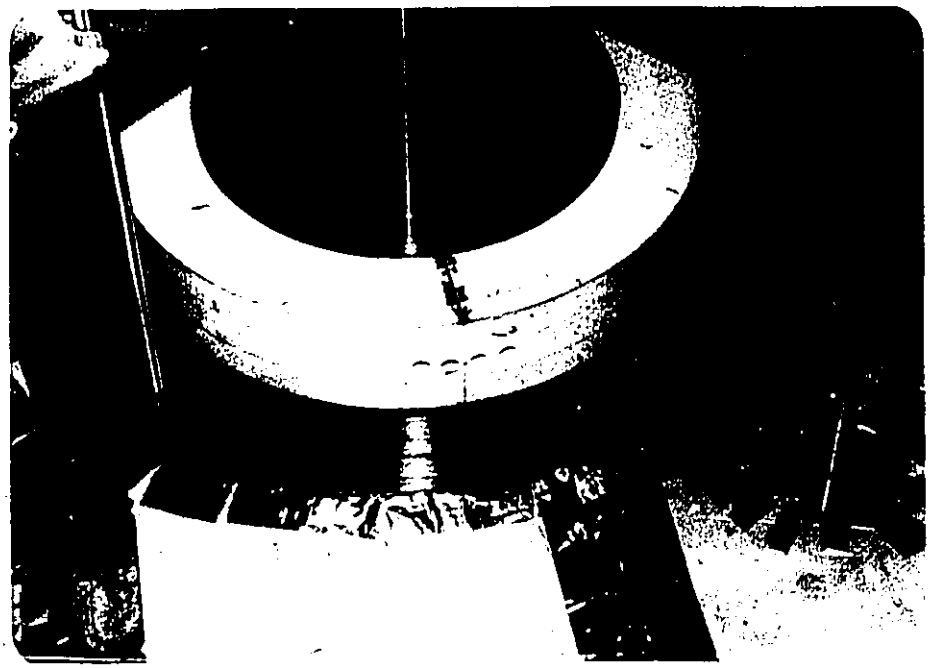

Figure 6.11: Assembly of the FW1 Rotor.

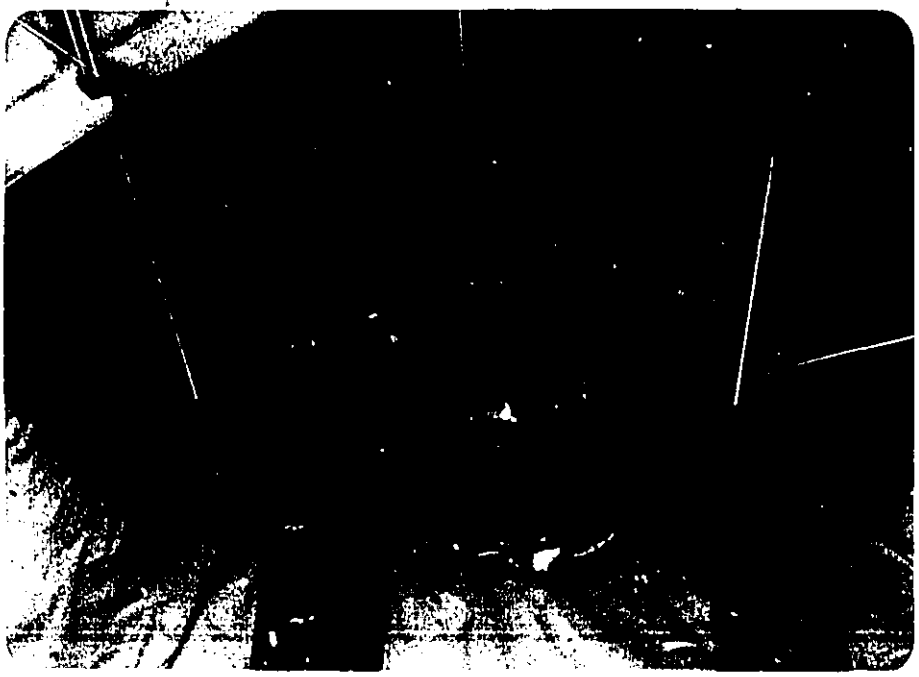

Figure 6.12: Assembly of the FW2 Rotor.

6.3.2 Concentricity

In attempting to render the arbour target areas concentric to each other and to the carbon ring outside diameter, the arbours were ground after the final assemblies of FW1 and FW2. The attempts on each rotor failed, resulting in the following mechanical runouts.

For FW1;

1. Top arbour 2,2 mils @ 112 degrees.
2. bottom arbour 7,0–8,0 mils @ 292 degrees.

For FW2;

1. Top arbour 2,8 mils @ 250 degrees.
2. Bottom arbour 2,8 mils @ 250 degrees.

These results were obtained by installing the rotors in a vertical milling machine and adjusting them to ensure that the quill shaft bores were running concentric to within +–0,0001". The top and bottom target areas' mechanical and electrical runouts were then measured station by station, every 45 degrees, using a Mitutoyo Digimatic Indicator type ID–150ME and an oppositely mounted Bently Nevada series 7200 proximity probe as shown in Figure 6.13 and in Figure 6.14. FW1's lower arbour suffered the most from this attempted corrective measure.

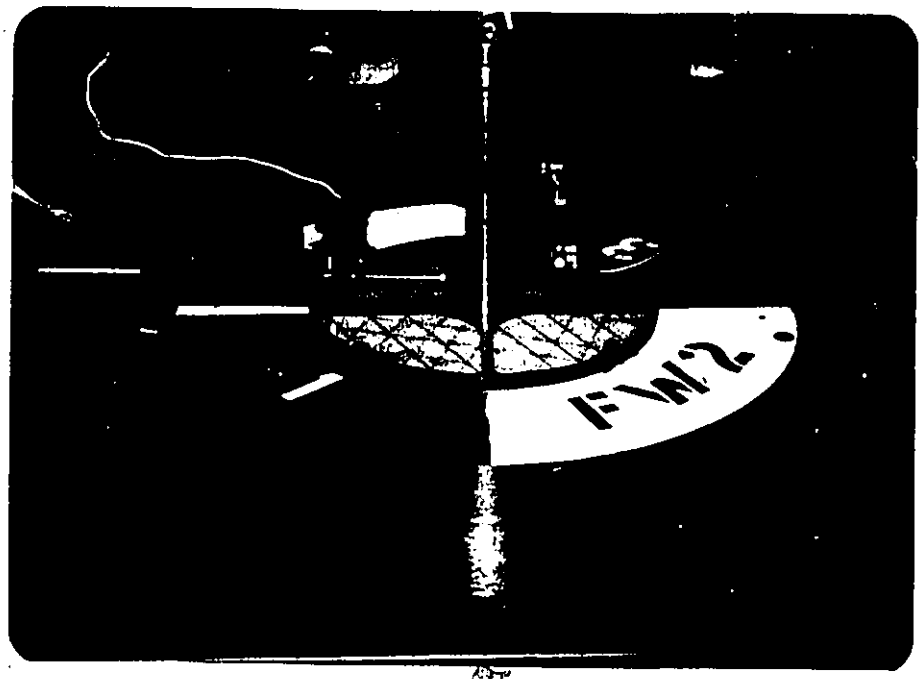

Figure 6.13: Post Grinding Concentricity Verification on FW2, Top View.

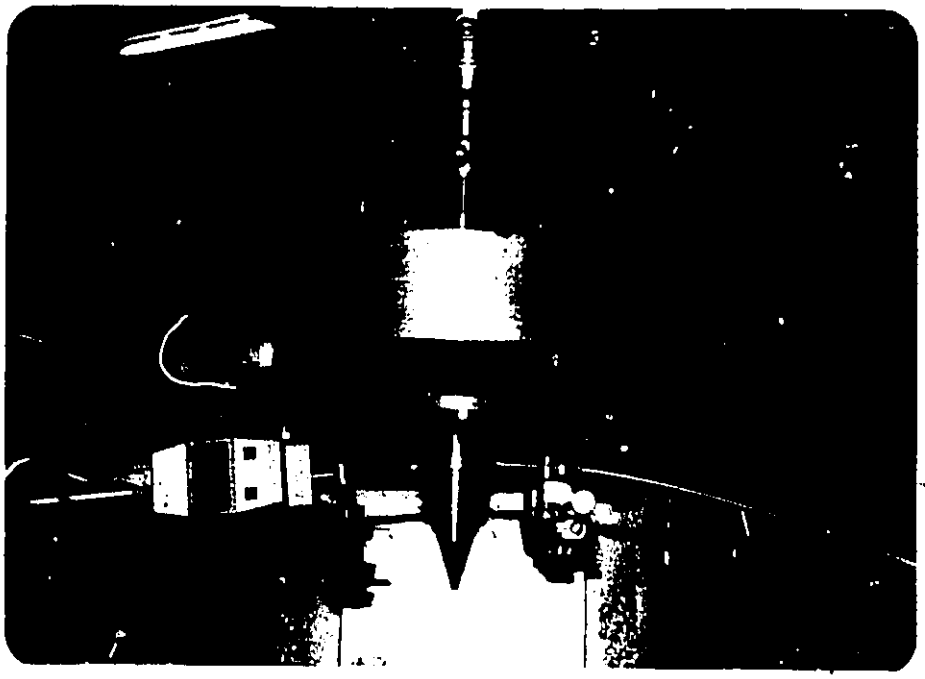

Figure 6.14: Post Grinding Concentricity Verification on FW2, Bottom View.

1.4 *Methods of Balance*

Balance correction of the composite hub flywheels was more involved than the metal hub flywheels since any alteration brought to the rotors was permanent. The static imbalance could usually be adjusted solely by removing equal amounts of material from the composite hub in each plane, or when the correction warranted it, by through drilling. Because the couple imbalances were quite large, they were corrected by cementing cylindrical plugs of brass or copper in the hubs, as shown in Figure 6.15 for FW2. The holes were drilled 1 inch from the hub-ring interface and had a maximum diameter of 3/8 of an inch. Based on analyses of radial position and hole-size effects in composite discs [32], this practice was determined to be suitable in that it would not reduce the structural integrity of the hub. Further, R.S. Steele [49] demonstrated that holes drilled near the outer diameter of a disk type composite hub flywheel did not appear to affect its ultimate speed capability. Our in house testing of composite discs also supported the above.

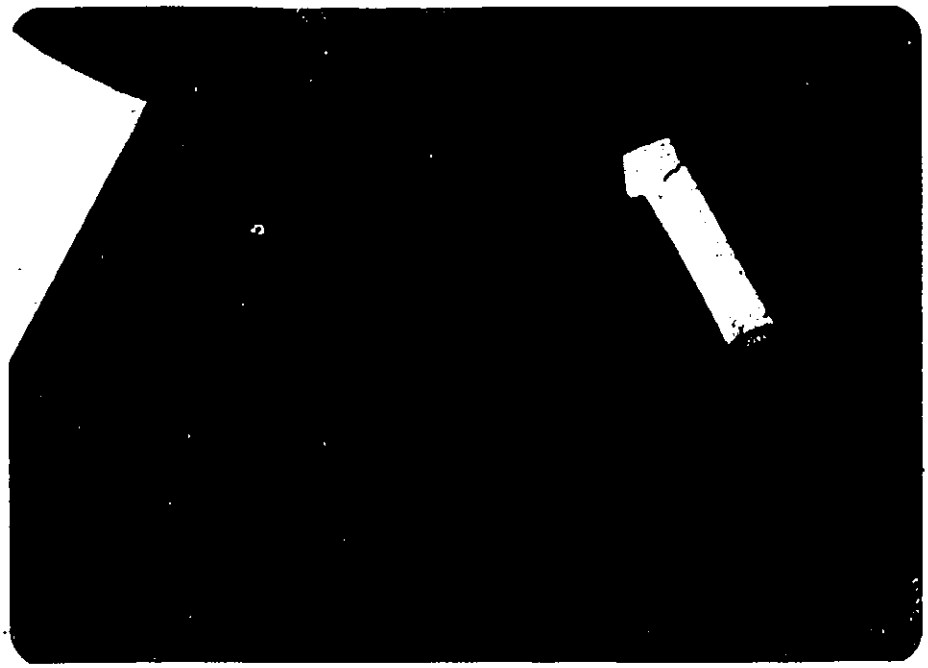

Figure 6.15: Composite Hub Flywheel Balance Correction. To the Left is a Static Correction Through Mass Removal and to the Right is One of a Pair of Weights for a Dynamic Correction.

6.2 *Metal Hub Rotors*

6.2.1 *Component Balance*

As determined in section 6.2, the wet-filament-wound composite rings do not possess any appreciable amount of static imbalance. Further, it could be noted that these rings cannot be balanced as individual components as balance corrections cannot be made directly to the rings. Also, the metallic components (hubs and arbours) were machined to exacting tolerances and were subjected to rigorous 'in-house' inspection prior to acceptance. Thus, the metallic hub rotors do not lend to, nor should they require, any component balance prior to assembly.

6.2.2 *Methods of Balance*

Balancing the assembled metal hub flywheels consisted of applying correction weights (aluminum tape and lead) on the inside diameter of the hubs. On the flex-rim hub rotors, the weights where distributed at 45 degrees away from the spokes to minimize the loading in these high stress regions. The balance correction weights were comprised of a static component positioned at mid-span axially, and equal and opposite weights applied on the top and bottom of the hub inside diameter to correct for the couple imbalance, as shown in Figure 6.16 for the FW3 flywheels.

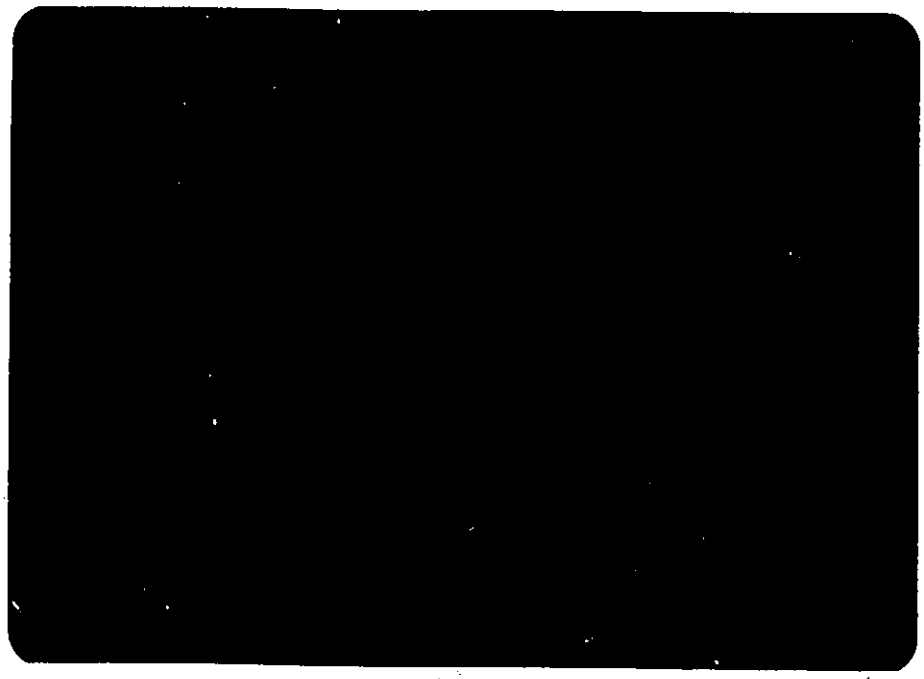

Figure 6.16: Metal Hub Balance. Shown are a Static Correction Weight and one of a Pair of Opposing Dynamic Correction Weights.

Chapter VII
ROTOR STATE-OF-BALANCE EVALUATION

Many tests were performed prior to the full development of the balancing procedure. However, the key balance data are listed in Table 3 for each of the rotors tested. An observation worth noting is that for each composite hub rotor design, the dynamic responses (filtered vibration amplitudes) on the way down from the maximum speeds attained always differed from the runup responses for the first few runs. Not only did the rotor's state-of-balance (mass center) change with speed, as was observed by R.S. Steele [46], and in experiment FW3A-BD-6, but the changes were permanent.

FW1 reached its permanently strained or seated configuration after its second test to maximum or design speed where the vibration response became highly repeatable. Figure 7.1 shows the dynamic response of FW1 after test #6. The growth in plane 2 is attributed to the mechanical runout of the lower arbour, induced from the concentricity grinding. Because of the arbour center of gravity shift, dynamic loading from high speed testing is sufficient to pull against the flex-ring attachment giving rise to a lower plane amplitude increase proportional to the square of the spin velocity. The phase angle over the whole range was steady at 290 degrees, corresponding exactly to the measured mechanical runout in the milling machine setup, described earlier.

FW2 required four tests to gradually bring it to its maximum operational design speed. After the fourth test which brought the rotor to a maximum

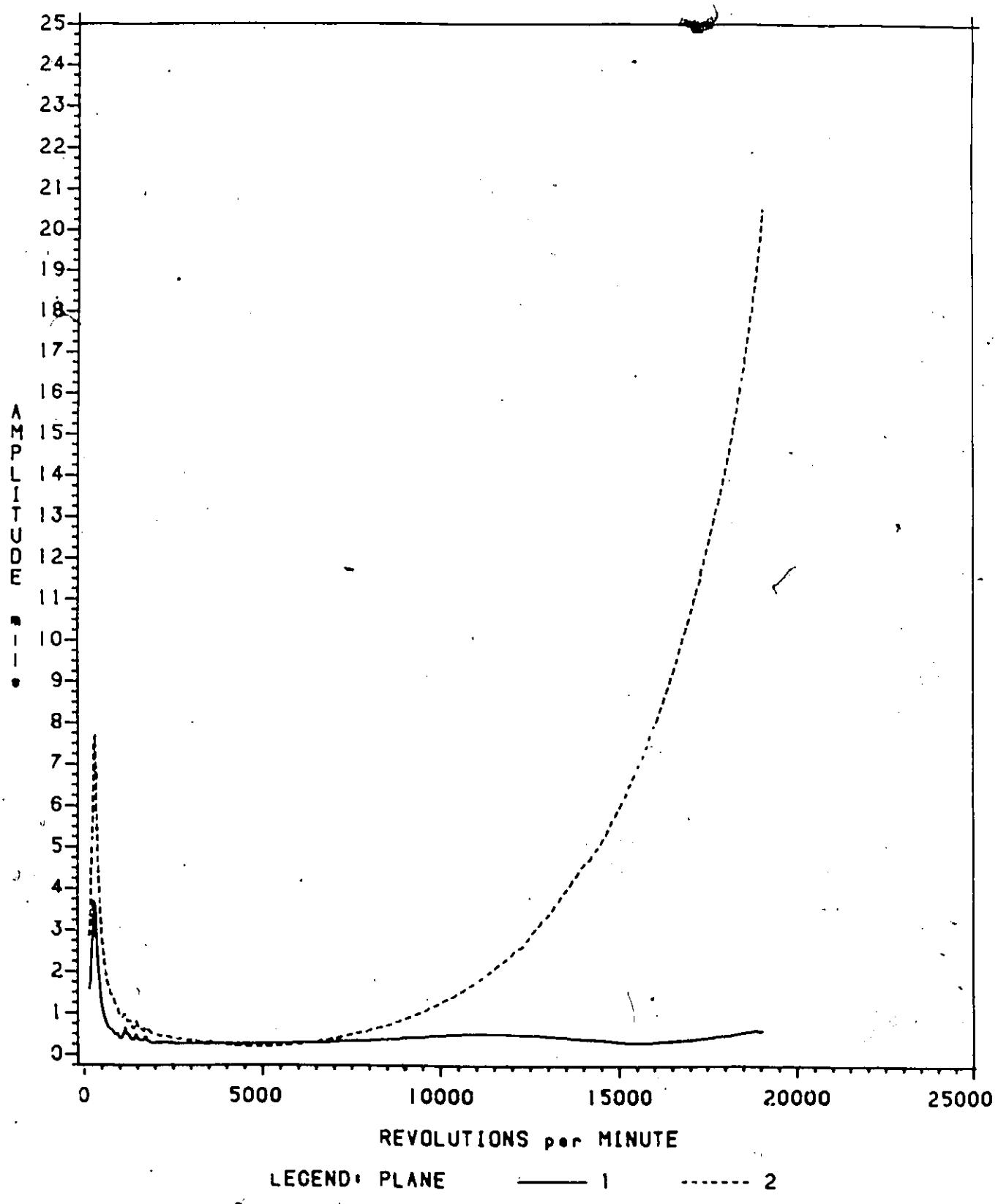

Figure 7.1: Repeatable Dynamic Response of Rotor FW1.

stressing, it still showed a small difference in pre- and post-test dynamic response, indicating that some seating or mass migration was still occurring.

FW3 did not show any signs of permanent mass shifting or seating effect. Although test FW3-1 ended in a failed carbon ring [32] leaving no post-test dynamic response data, a reconstructed rotor, FW3-2, had a repeatable response from its first test.

FW4 was not subjected to high-speed testing. After FW4's initial hub assembly, the rotor indicated a tilt of 6'52" (0.115 degree) and a radial eccentricity of 15.75 mils when installed in the vacuum chamber. The large correction weights required for balancing vetoed any further attempts to balance the rotor. Thus, FW4 was removed from the vacuum chamber, disassembled, and a dimensional tolerance was conducted.

The only tolerance discrepancies observed were on the central bushing and on the dowel pin hole locations in the central bushing and spring spoke plates. The central bushing registered a 3.5 mils runout on the top centering boss and a 2'52" (0.047 degree) tilt on the top surface against which the spring spoke plate rests. The runout and tilt location were separated by 135 degrees. The bushing was remachined to specification thus loosing the top boss' use in centering the spring spoke plate. Upon reassembly, the spring spoke plates were matched to the central bushing by having three dowel pin holes from each component match the corresponding holes in the central bushing.

Once reassembled and reinstalled in the vacuum chamber the assembly indicated a tilt of 16'37" (0.277 degree) and a radial eccentricity of 7 mils, halting any further attempts in testing the rotor.

Several observations of interest can be made with respect to the initial correction weight magnitudes required for each rotor design.

1. For FW1-1, the initial static correction (42.0 g-cm/340 deg.) is out of phase with that made to the hub prior to assembly (349.5 g-cm/170 deg.) indicating that slightly more material was removed than what was required at that time. Thus, the total static imbalance in the SMC hub was in the order of 308.3 g-cm. By comparison, the total static imbalance in rotor FW3-1 was 103.4 g-cm.

2. The initial balance of rotor FW2-1 required a significant static correction of 817.9 g-cm at 153 deg. Again this correction was out of phase with the correction made to the hub prior to assembly. However, as was discussed in section 6.3.1 the S2-laminated hub was not so much out of balance as originally perceived. From the combined data, the actual imbalance in this hub was in the order of 197.1 g-cm.

3. Rotor FW3-1 required the least amount of balance relative to the other rotors considering that this rotor was assembled without any component prebalance. Further, the flex-rim hub was removed from this rotor after ring failure occurred (moderately rough treatment) and used in rotors FW3-2 and FW3-3. This hub received some damage during the failure sequence which accounts for the increased imbalance of the latter two rotors. Also, both FW3-2 and FW3-3 were balanced under evacuated conditions resulting in a much higher precision balance over FW3-1 as evidenced by the residual amplitudes.

Table 3

Balance Data for the Final Rotors

ROTOR/TEST	CORRECTION WEIGHTS		BALANCE SPEED (rpm)	RESIDUAL AMPLITUDES AT BALANCE SPEED				MAXIMUM SPEED (rpm)
				PRETEST		POST-TEST		
	STATIC (g/cm)	COUPLE (g-cm²)		PLANE 1	PLANE 2	PLANE 1	PLANE 2	
FW1-1/1	42.0/340	-	3,000	0.6/182	0.6/002	1.1/190	1.8/27	19,000
/2	1.4/285	-	13,000	2.2/187	2.5/027	-	-	19,000
/3	66.7/127	653.2/225 653.2/45	3,000	1.4/246	3.5/327	1.4/246	3.5/327	18,450
/4	-	-	3,000	1.7/245	3.9/320	1.5/244	4.1/317	18,830
/5	160.0/105	2552.1/126 2552.1/305	3,000	0.3/PH[3]	0.5/PH	0.1/PH	0.8/280	19,035
/6	7.0/296	Note 4	3,000	0.2/PH	0.2/PH	-	-	19,000
/7	Note 4	Note 4	-	-	-	-	-	19,042
/8	Note 4	Note 4	-	-	-	-	-	15,000
FW2-1/1	817.9/153	-	3,000	1.1/298	1.1/118	1.4/317	1.3/95	16,300
/2	43.3/173	1742.4/352 1794.1/175	3,000	0.0/PH	0.2/PH	1.1/285	1.1/300	18,750
/3	87.3/187	456/102 456/282	3,000	1.0/197	0.9/022	3.4/355	3.0/353	22,000
/4	107.3/0	288/092 288/277	3,000	0.4/102	1.2/165	0.7/109	1.4/255	24,787
FW3-1/1	103.4/116	493.6/141 474.6/323	1,500	0.9/300	2.3/320	-	-	21,398
FW3-2/1	303.4/141	1680.2/142 1680.2/322	3,000	0.2/PH	0.4/PH	0.2/PH	0.4/PH	20,000
Note 5	-	-	-	-	-	-	-	-
FW3-3/1	300.6/94	1142.3/171 1142.3/343	3,000	0.4/209	0.6/86	-	-	21,345

Notes: 1. Static correction weights are given as: correction (g-cm)/phase angle (degrees). Dynamic corrections are given for planes 1 and 2, respectively, as: correction (g-cm²)/phase angle (degrees).
2. Amplitude vectors are given as: amplitude (mils)/phase angle (degrees).
3. 'PH' designates "Phase Held", i.e., the amplitude was too low for the DVF to compute a phase angle.
4. No balance required.
5. Rotor FW3-2 was extensively tested and used for all of the dynamic experiments.

Chapter VIII
CONCLUSIONS

A high speed, precision balance laboratory was established in conjunction with the spin test facility development [32]. The rotor dynamics monitoring equipment was also used for precision rotor balancing.

The static/couple derivation together with slow-roll compensation was shown to be an effective precision balance technique and allowed for experimental investigations to be performed on rotor induced motion. This includes the experimentally evaluated moment induced retrograde whirl and change in rotor balance status with speed as well as system induced motion such as resonant oil whip. By allowing to discretize each rotor dynamic phenomena, the test engineer was provided with the diagnostic knowledge for proper interpretation of the dynamic responses encountered during rotor spin tests.

The conclusion to be drawn from the balance data is that the composite-hub rotors experienced mass shifting during the first several runs to design speed. It is believed that this shifting resulted from component 'seating' between the FRA and the rotor, not from hub material migration. Once seated, however, they became very repeatable as experienced with FW1. Thus, from both the balancing and state-of-balance retention points of view, rotor design FW3 is clearly the most desirable.

Appendix A
BALANCING PROGRAM -STATIC2-

Static Balance Computer Program for Overhung Rotors, written for a Hewlett-Packard 41C or 41CV programmable calculator.

Once the program execution is initiated, it is designed to stop and ask for each input value by an alphanumeric prompt. After each input the R/S key is pressed to resume program execution.

There is a total of ten prompts to key in the required data for balancing, followed by five more prompts if trim balancing is desired. The alphanumeric prompts for initial balance are:

1. "AMP1 AS IS?" – Amplitude at probe #1 as is
2. "PHASE1 AS IS?" – As is phase angle at probe #1
3. "AMP2 AS IS?" – Amplitude at probe #2 as is
4. "PHASE2 AS IS?" – As is phase angle at probe #2
5. "TRIAL WEIGHT?" – Trial weight value, located at mid-span axially
6. "TRIAL ANGLE?" – Angular location of the trial weight
7. "AMP1 TRIAL?" – Amplitude at probe #1 with the trial weight
8. "PHASE1 TRIAL?" – Phase angle at probe #1 with the trial weight
9. "AMP2 TRIAL?" – Amplitude at probe #2 with the trial weight
10. "PHASE2 TRIAL?" – Phase angle at probe #2 with the trial weight

Pressing the R/S key after keying in the last input value will begin the program execution and the "program execution annunciator symbol" will appear

on the display and will travel from left to right until the computed correction weight is displayed. The angular location of the correction weight is displayed by pressing the R/S key once more.

If the after balance dynamic response is not exactly as desired, trim balancing will provide the final correction.

Pressing the R/S key will yield the "TRIM BALANCE" display indicating that the program is at this stage of its execution. Pressing the R/S key again will put the calculator in the data input mode for trim balance and the program is again designed to stop and ask for each input value, measured at balance speed. The alphanumeric prompts for trim balance are:

1. "RES AMP1?" – Residual amplitude at probe #1 after initial balance
2. "RES PHS1?" – Corresponding phase at probe #1
3. "RES AMP2?" – Residual amplitude at probe #2 after initial balance
4. "RES PHS2?" – Corresponding phase at probe #2

Pressing the R/S key after keying in the last data input value will begin the execution of the trim balance portion of the program and the "program execution annunciator symbol" will again appear on the display and travel from left to right until the computed trim correction weight is displayed. The angular location of the correction weight is displayed by pressing the R/S key one last time.

This routine was successfully verified in the laboratory.

A listing of the computer program is contained in the following five pages.

Note. Whenever quotation marks (") appear around a character or a string of characters, these characters should be keyed in as alphanumeric characters.

The asterisk is only a visual aid to help the reader locate labels in the program listing.

```
01  *LBL "STATIC2"
02  AMP1 AS IS ?"
03  PROMPT
04  STO 00
05  "PHASE1 AS IS ?"
06  PROMPT
07  STO 01
08  "AMP2 AS IS ?"
09  PROMPT
10  STO 02
11  "PHASE2  AS IS ?"
12  PROMPT
13  STO 03
14  "TRIAL WEIGHT ?"
15  PROMPT
16  STO 04
17  "TRIAL ANGLE ?"
18  PROMPT
19  STO 05
20  "AMP1 TRIAL ?"
21  PROMPT
22  STO 06
23  "PHASE1 TRIAL ?"
24  PROMPT
25  STO 07
26  "AMP2 TRIAL ?"
27  PROMPT
28  STO 08
29  "PHASE2 TRIAL ?"
30  PROMPT
31  STO 09
32  XEQ "W10"
33  XEQ "W20"
34  XEQ "CADD"
35  STO 00
```

```
36  X <> Y
37  STO Ø1
38  XEQ "W11"
39  XEQ "W21"
4Ø  XEQ "CADD"
41  STO Ø6
42  X <>  Y
43  STO Ø7
44  XEQ "W1Ø"
45  XEQ "W11"
46  XEQ "CSUB"
47  XEQ "WTW"
48  XEQ "CDIV"
49  STO Ø4
5Ø  X <> Y
51  STO Ø5
52  XEQ "W1Ø"
53  XEQ "W11"
54  XEQ "CDIV"
55  XEQ "DISP"
56  STOP
57  "TRIM BALANCE"
58  PROMPT
59  "RES AMP1 ?"
6Ø  PROMPT
61  STO ØØ
62  "RES PHS1 ?"
63  PROMPT
64  STO Ø1
65  "RES AMP2 ?"
66  PROMPT
67  STO Ø2
68  "RES PHS2 ?"
69  PROMPT
7Ø  STO Ø3
71  XEQ "W1Ø"
```

```
 72  XEQ "W2Ø"
 73  XEQ "CADD"
 74  XEQ "WTW"
 75  XEQ "CDIV"
 76  XEQ "DISP"
 77  STOP
 78  *LBL "W1Ø"
 79  RCL Ø1
 80  RCL ØØ
 81  RTN
 82  *LBL "W2Ø"
 83  RCL Ø3
 84  RCL Ø2
 85  RTN
 86  *LBL "W11"
 87  RCL Ø7
 88  RCL Ø6
 89  RTN
 9Ø  *LBL "W21"
 91  RCL Ø9
 92  RCL Ø8
 93  RTN
 94  *LBL "WTW"
 95  RCL Ø5
 96  RCL Ø4
 97  RTN
 98  *LBL "CADD"
 99  P-R
1ØØ  X <> 4
1Ø1  RDN
1Ø2  RDN
1Ø3  P-R
1Ø4  R↑
1Ø5  +
```

```
106  RDN
107  +
108  R↑
109  R-P
110  RTN
111  *LBL "CSUB"
112  P-R
113  CHS
114  X <> Y
115  CHS
116  RDN
117  RDN
118  P-R
119  R↑
120  +
121  RDN
122  +
123  R↑
124  R-P
125  RTN
126  *LBL "CDIV"
127  1/X
128  X <> Y
129  CHS
130  RDN
131  *
132  RDN
133  +
134  R↑
135  RTN
136  *LBL "DISP"
137  "COR. WGHT = "
138  ARCL X
139  AVIEW
```

```
140  STOP
141  "ANGLE = "
142  ARCL Y
143  AVIEW
144  RTN
145  END
```

Appendix B
BALANCING PROGRAM -BALANCE-

Two Plane Rigid Rotor Balance Computer Program written for the Hewlett-Packard 41C or 41CV calculator.

With the exception of the "trim balance" feature, the program was prepared by Paul Y. Kim in June, 1980 as a Laboratory Memorandum for the National Research Council of Canada, Division of Mechanical Engineering, Engine Laboratory section, Ottawa, Canada.

The following program use description was taken from P.Y. Kim's memorandum.

The calculator is programmed to stop and ask for each input value by an alphanumeric prompt.

After pressing the ON key to turn on the calculator, the following keys should be pressed in the order listed:

1. XEQ
2. ALPHA
3. B A L A N C E
4. ALPHA

1. The first prompt is "AMP1 AS IS?". This means that the calculator is ready to accept the input value of the "amplitude #1 as is", that is, ONLY the amplitude value (not the phase angle) of the original unbalance response at the probe #1. Key in the value, then press the R/S key. After keying in each input value, the key R/S should be pressed to resume the calculation.

2. The second prompt is "AMP2 AS IS?". Key in the amplitude value, not the phase angle, of the original unbalance response at the probe #2, then press the key R/S.

3. The third prompt is "TRIAL WEIGHT1?". Key in the weight of the first trial weight at the balancing plane #1, then press the key R/S.

4. Similarly, the next five prompts are:

1. "AMP1 TRIAL1 ?"
2. "AMP2 TRIAL1 ?"
3. "TRIAL WEIGHT2 ?"
4. "AMP1 TRIAL2 ?"
5. "AMP2 TRIAL2 ?"

They mean "Please key in the values of":

1. Amplitude at probe #1 with the trial weight at plane #1,
2. Amplitude at probe #2 with the trial weight at plane #1,
3. Trial weight at the balancing plane #2,
4. Amplitude at probe #1 with the trial weight at plane #2,
5. Amplitude at probe #2 with the trial weight at plane #2, respectively.

5. The next five prompts as for the phase angles:

1. "PHASE1 AS IS ?"
2. "PHASE2 AS IS ?"
3. "TRIAL ANGLE1 ?"
4. "PHASE1 TRIAL1 ?"
5. "PHASE2 TRIAL1 ?"
6. "TRIAL ANGLE2 ?"
7. "PHASE1 TRIAL2 ?"
8. "PHASE2 TRIAL2 ?"

The unit of phase angle is "degree". Corresponding values to be keyed in after each prompt listed above are:

1. The value of original or "as is" phase angle at probe #1,
2. The value of original or "as is" phase angle at probe #2,
3. Phase angle of the trial weight at balancing plane #1,
4. Phase angle at probe #1 with trial weight at plane #1,
5. Phase angle at probe #2 with trial weight at plane #1,
6. Phase angle of the trial weight at balancing plane #2,
7. Phase angle at probe #1 with trial weight at plane #2,
8. Phase angle at probe #2 with trial weight at plane #2, respectively.

After keying in all the values, one at a time followed by the R/S key, the "program execution symbol" will appear on the display and will travel from the left end to the right end of the display. The motion of the "program execution symbol" on the display of the calculator means that the program is being executed. After the symbol traverses the display approximately five times from left to right, the first computed correction weight is displayed. After the figures stop in the display, the R/S key should be pressed to proceed to the next computed correctional weight.

Trim balance is performed in the same fashion as for static balance with the exception that the R/S key has to be pressed two more times to obtain the lower plane correction information.

A listing of the computer program is contained in the following nine pages.

Note: Whenever quotation marks (") appear around a character ar a string of characters, these characters should be keyed in as alphanumeric characters. The asterisk is only a visual aid to help the reader locate labels in the program listing

```
01  *LBL "BALANCE"
02  "AMP1 AS IS ?"
03  PROMPT
04  STO 01
05  "AMP2 AS IS ?"
06  PROMPT
07  STO 02
08  "TRIAL WEIGHT1 ?"
09  PROMPT
10  STO 03
11  "AMP1 TRIAL1 ?"
12  PROMPT
13  STO 04
14  "AMP2 TRIAL1 ?"
15  PROMPT
16  STO 05
17  "TRIAL WEIGHT2 ?"
18  PROMPT
19  STO 06
20  "AMP1 TRIAL2 ?"
21  PROMPT
22  STO 07
23  "AMP2 TRIAL2 ?"
24  PROMPT
25  STO 08
26  "PHASE1 AS IS ?"
27  PROMPT
28  STO 11
29  "PHASE2 AS IS ?"
30  PROMPT
31  STO 12
32  "TRIAL ANGLE1 ?"
33  PROMPT
34  STO 13
35  "PHASE1 TRIAL1 ?"
```

```
36  PROMPT
37  STO 14
38  "PHASE2 TRIAL1 ?"
39  PROMPT
40  STO 15
41  "TRIAL ANGLE2 ?"
42  PROMPT
43  STO 16
44  "PHASE1 TRIAL2 ?"
45  PROMPT
46  STO 17
47  "PHASE2 TRIAL2 ?"
48  PROMPT
49  STO 18
50  XEQ "W11"
51  XEQ "W10"
52  XEQ "CSUB"
53  XEQ "T1"
54  XEQ "CDIV"
55  STO 21
56  X <> Y
57  STO 31
58  XEQ "W21"
59  XEQ "W20"
60  XEQ "CSUB"
61  XEQ "T1"
62  XEQ "CDIV"
63  STO 22
64  X <> Y
65  STO 32
66  XEQ "W12"
67  XEQ "W10"
68  XEQ "CSUB"
69  XEQ "T2"
70  XEQ "CDIV"
```

```
71  STO 23
72  X <> Y
73  STO 33
74  XEQ "W22"
75  XEQ "W2Ø"
76  XEQ "CSUB"
77  XEQ "T2"
78  XEQ "CDIV"
79  STO 24
8Ø  X <> Y
81  STO 34
82  XEQ "ALPHA12"
83  XEQ "ALPHA21"
84  XEQ "CMULT"
85  STO 29
86  X <> Y
87  STO 39
88  XEQ "ALPHA11"
89  XEQ "ALPHA22"
9Ø  XEQ "CMULT"
91  RCL 39
92  RCL 29
93  XEQ "CSUB"
94  STO 25
95  X <> Y
96  STO 35
97  XEQ "ALPHA22"
98  XEQ "W1Ø"
99  XEQ "CMULT"
1ØØ STO 26
1Ø1 X <> Y
1Ø2 STO 36
1Ø3 XEQ "ALPHA12"
1Ø4 XEQ "W2Ø"
1Ø5 XEQ "CMULT"
```

```
106  RCL 36
107  RCL 26
108  XEQ "CSUB"
109  XEQ "DENOM"
110  XEQ "CDIV"
111  XEQ "UC1"
112  STOP
113  XEQ "ALPHA11"
114  XEQ "W20"
115  XEQ "CMULT"
116  STO 27
117  X <> Y
118  STO 37
119  XEQ "ALPHA21"
120  XEQ "W10"
121  XEQ "CMULT"
122  RCL 37
123  RCL 27
124  XEQ "CSUB"
125  XEQ "DENOM"
126  XEQ "CDIV"
127  XEQ "UC2"
128  STOP
129  *LBL "TRIM BALANCE"
130  PROMPT
131  "RES AMP1 ?"
132  PROMPT
133  STO 40
134  "RES AMP2 ?"
135  PROMPT
136  STO 41
137  "RES PHASE1 ?"
138  PROMPT
139  STO 42
140  "RES PHASE2 ?"
141  PROMPT
```

```
142  STO 43
143  XEQ "ALPHA22"
144  XEQ "RES1"
145  XEQ "CMULT"
146  STO 26
147  X <> Y
148  STO 36
149  XEQ "ALPHA12"
15Ø  XEQ "RES2"
151  XEQ "CMULT"
152  RCL 36
153  RCL 26
154  XEQ "CSUB"
155  XEQ "DENOM"
156  XEQ "CDIV"
157  XEQ "RES UC1"
158  STOP
159  XEQ "ALPHA11"
16Ø  XEQ "RES2"
161  XEQ "CMULT"
162  STO 27
163  X <> Y
164  STO 37
165  XEQ "ALPHA21"
166  XEQ "RES1"
167  XEQ "CMULT"
168  RCL 37
169  RCL 27
17Ø  XEQ "CSUB"
171  XEQ "DENOM"
172  XEQ "CDIV"
173  XEQ "RES UC2"
174  RTN
175  *LBL "CDIV"
176  1/X
177  X <> Y
```

```
178  CHS
179  GTO ØØ
18Ø  *LBL "CMULT"
181  X <> Y
182  *LBL ØØ
183  RDN
184  *
185  RDN
186  +
187  R↑
188  GTO Ø2
189  *LBL "CSUB"
19Ø  P-R
191  CHS
192  X <> Y
193  CHS
194  RDN
195  RDN
196  P-R
197  R↑
198  +
199  RDN
2ØØ  +
2Ø1  R↑
2Ø2  R-P
2Ø3  *LBL Ø2
2Ø4  RTN
2Ø5  *LBL "UC1"
2Ø6  "UC1 = "
2Ø7  GTO Ø1
2Ø8  *LBL "UC2"
2Ø9  "UC2 = "
21Ø  *LBL "Ø1"
211  ARCL X
212  " |- GRAMS,"
```

```
213  AVIEW
214  STOP
215  ARCL Y
216  " |- DEG"
217  AVIEW
218  RTN
219  *LBL "W11"
220  RCL 14
221  RCL Ø4
222  RTN
223  *LBL "W1Ø"
224  RCL 11
225  RCL Ø1
226  RTN
227  *LBL "W12"
228  RCL 17
229  RCL Ø7
230  RTN
231  *LBL "W21"
232  RCL 15
233  RCL Ø5
234  RTN
235  *LBL "W22"
236  RCL 18
237  RCL Ø8
238  RTN
239  *LBL "W2Ø"
240  RCL 12
241  RCL Ø2
242  RTN
243  *LBL "T1"
244  RCL 13
245  RCL Ø3
246  RTN
247  *LBL "T2"
```

```
248  RCL 16
249  RCL Ø6
25Ø  RTN
251  *LBL "ALPHA11"
252  RCL 31
253  RCL 21
254  RTN
255  *LBL "ALPHA12"
256  RCL 33
257  RCL 23
258  RTN
259  *LBL "ALPHA21"
26Ø  RCL 32
261  RCL 22
262  RTN
263  *LBL "ALPHA22"
264  RCL 34
265  RCL 24
266  RTN
267  *LBL "DENOM"
268  RCL 35
269  RCL 25
27Ø  RTN
271  *LBL "RES1"
272  RCL 42
273  RCL 40
274  RTN
275  *LBL "RES2"
276  RCL 43
277  RCL 41
278  RTN
279  *LBL "RES UC1"
28Ø  "RES UC1="
281  GTO Ø1
282  *LBL "RES UC2"
```

```
283  "RES UC2="
284  GTO Ø1
285  END
```

BIBLIOGRAPHY

CRM refers to_ Contractors' Review Meeting, annual symposia to share results of the previous year's work with each other and the sponsoring agency, the US Department of Energy.

1. Akkok, K. and McCEttles, C.M., The Onset of Whirl Instability in Journal Bearings of Various Bore Shapes and Groove Sizes; Journal of Lubrication Technology, Trans. of the ASME, Vol. 105, July 1983.
2. Andeen, G.B., Approach to Flywheel Development; Stanford Research Institute, Proceedings of the 1975 Flywheel Technology Symposium.
3. Babelay, E.F. Jr., Rotor Testing in FY 82; CRM 1982, p.274.
4. Bert, C.W. and Ramunujam, G., Design Guide for Composite-Material Flywheels; Rotor Dynamic Considerations Part 1- System Whirling and Stability; University of Oklahoma, September 1981, Final Report on Subcontract No. 6448509, Performed Under The Auspices of the U.S. Department of Energy Under Contract W-7405-Eng-48.
5. Bishop, R.E.D., An Introduction to the Balancing of Flexible Rotors; Engineering Materials and Design, Vol.9, 1966, pp.1468-1474.
6. Boeker, G.F. and Sternlicht, B., Investigation of Translatory Fluid Whirl in Vertical Machines; Journal of Applied Mech., Trans. of the ASME, Jan. 1956, pp. 13-19.
7. Chen, T.L.C. and Bert, C.W., Whirling Response and Stability of Flexibly Mounted, Ring-Type Flywheel Systems; Journal of Mechanical Design, April 1980, Vol.102, pp.369-378.

8. Dostal, M., Roberts, J.B. and Holmes, R., Stability Control of Flexible Shafts Supported on Oil-Film Bearings; Journal of Sound and Vibration (1974) 35(3), 361-377.

9. Dowson, D. and Taylor, C.M., The State of Knowledge in the Field of Bearing Influenced Rotor Dynamics; Tribology International, October 1980, volume 13, number 5.

10. Enrich, F. and Childs, D., Self-Excited Vibration in High-Performance Turbomachinery; Mechanical Engineering, May 1984, Vol. 106, Number 5, pp.66-79.

11. Fleming, D.P., Rotor-Bearing Dynamics of Modern Turbomachinery; Tribology International, October 1980, volume 13, number 5.

12. Frank, A. A. and Beachley, N. H., Control-Strategy Study for a Heat-Engine/Flywheel/Continuously-Variable-Transmission Vehicle; CRM 1981.

13. Genta, G., Spin Test on Medium Energy Density Flywheels; Composites, Vol. 13, January 1982, pp.38-46.

14. Goodman, T.P., A Least-Squares Method for Computing Balance Corrections; Journal of Engineering for Industry, Trans. ASME, Series B, Vol. 86, No. 3, August 1964, pp.273-279.

15. Gunter, E.J. and Barrett, L.E. and Allaire, P.E., Design of Nonlinear Squeeze-Film Dampers for Aircraft Engines; Journal of Lubrication Technology, Trans. of the ASME, Jan. 1977, pp. 57-64.

16. Den Hartog, J.P., Mechanical Vibrations; 4th edition, McGraw-Hill, 1956, pp.253-265 295-299.

17. Holmes, R., The Role of Oil-Film Bearings in Promoting Shaft Instability and the Remedial Effect of Damping; Tribology International, Vol. 13, No. 5, October 1980.

18. Flanagan, R.C., Program Overview and Diesel/Flywheel Hybrid Power Train Design; Proceedings IECEC '82 the 17th Intersociety Energy Conversion Engineering Conference, August 1982, pp. 1955–1960, Los Angeles, CA.

19. Flanagan, R.C., Wong, J., and Munro, M., Fibre Composite Rotor Selection and Design; Proceedings IECEC '82 the 17th Intersociety Energy Conversion Engineering Conference, August 1982, pp. 1961–1966, Los Angeles, CA.

20. Munro, M., Miyase, A., McCrea, J. and Flanagan, R.C., Manufacture and Testing of Fibre Composite Rotor Components; Proceedings IECEC '82 the 17th Intersociety Energy Conversion Engineering Conference, August 1982, pp.1967–1972, Los Angeles, CA.

21. International Standards, Balance Quality of Rotating Rigid Bodies; ISO 1940–1973(E).

22. Jackson, C., The Practical Vibration Primer; Gulf Publishing Company, second printing September 1981, ISBN 0–87201–891–0.

23. Kalns, I., Heat Engine/Flywheel Vehicle Drive Design Results and Analysis, Phase 1; CRM 1981.

24. Kim, P.Y., Review of Flexible Shaft Balancing Techniques; Sixth Machinery Dynamics Seminar on Vibration Standards and Current Techniques for Flexible Rotor Balancing, September 1980, Toronto, Ontario.

25. Kubo, L. H. and Forrest, L., Assessment of Flywheel System Benefits in Selected Vehicle Application; CRM 1981.

26. Lund, J. and Tonnesen, J., Analysis and Experiments on Multiplane Balancing of a Flexible Rotor; Journal of Engineering Industry, Trans. ASME, Vol.94, Series B, No. 1, February 1972, pp. 233–242.

27. Lund, J.W. and Thomsen K.K., A Calculation Method and Data for the Dynamic Coefficients of Oil–Lubricated Journal Bearings; ASME Design

Engineering Conference April 1978: Fluid Film Bearings in Rotating Machinery and Bearing Design Optimization.

28. Marchand, M.P., The Design and Fabrication of a Dynamic Balancing Facility; Fourth Year Thesis, University of Ottawa, April 1983.

29. Meriam, J.L., Engineering Mechanics Statics and Dynamics; John Wiley & Sons, Inc., 1980, ISBN 0-471-07862-X, pp. 451-458.

30. Meirovitch, L., Methods of Analytical Dynamics; McGraw-Hill Book Company, pp. 149-157.

31. Miller, K.A., Recent Spin Tests of Two Composite Wagon Wheel Flywheels; CRM 82, pp. 348-355.

32. Miller, P.A., High-Speed Testing and Spin-Test Facility Development; MASC Thesis, University of Ottawa, Department of Mechanical Engineering, 1986.

33. Mitchell, J.S., An Introduction to Machinery Analysis and Monitoring; PennWell Publishing Company, ISBN 0-87814-145-6, pp.257-259.

34. Morrison, D., Influence of Plain Journal Bearings on the Whirling Action of an Elastic Rotor; Proc. Instn. Mech. Engrs., Vol. 176, No. 22, 1962.

35. Muster, D. and Flores, B., Balancing Criteria and Their Relationship to Current American Practice; Journal of Engineering for Industry, November 1969, pp. 1035-1046.

36. Newkirk, B.L. and Lewis, J.F., Oil-Film Whirl -An Investigation of Disturbances Due to Oil Films in Journal Bearings; Journal of Applied Mechanics, Trans. of the ASME, January 1956.

37. Flanagan, R.C., Munro, M.B., Wong, J. and Miyase, A., Rotor Assessment and R & D Program Definition; Report No. UOME-FP-8301, NRC/DSS Contract No. OSU80-00043, Department of Mechanical Engineering, University of Ottawa, January 1983, 112 pp.

38. Munro, M.B., Miyase, A., Flanagan, R.C. and Bouchard, D., Basic Material Studies for Fibre Composite Flywheels; Report No. UOME-FP-8302-1, NRC/DSS Contract No. OSU80-00043, Department of Mechanical Engineering, University of Ottawa, January 1983, 59 pp.

39. Flanagan, R.C. and Wong, J., High Energy Density Fibre Composite Rotor Design and Analysis; Report No. UOME-FP-8303-1, NRC/DSS Contract No. OSU80-00043, Department of Mechanical Engineering, University of Ottawa, January 1983, 176 pp.

40. Munro, M.B., Miyase, A. and Flanagan, R.C., Advanced Materials and Manufacturing Studies for Fibre Composite Flywheels; Report No. UOME-FP-8304-1, NRC/DSS Contract No. OSU80-00043, Department of Mechanical Engineering, University of Ottawa, January 1983, 99 pp.

41. Flanagan, R.C., Miller, P., McCrea, J., Munro, M.B. and Wong, J., Design and Development of a High-Speed Spin Test Facility and Rotor Dynamic Testing; Report No. UOME-FP-8305-1, NRC/DSS Contract No. OSU80-00043, Department of Mechanical Engineering, University of Ottawa, January 1983, 54 pp.

42. Parszewski, Z. and Cameron, A., Oil Whirl of Flexible Rotors; Proc. Instn. Mech. Engrs., Vol. 176, No. 22, 1962.

43. Pinkus, O., Experimental Investigation of Resonant Whip; Journal of Applied Mechanics, Trans. ASME, July 1956, pp. 975-983.

44. Poritsky, H., Contribution to the Theory of Oil Whip; Journal of Applied Mechanics, Trans. ASME, August 1953. pp. 1153-1161.

45. Rabenhorst, D.W., Flywheel Technology Development at APL; CRM 1980, pp.386-392.

46. Steele, R.S., Composite Flywheel Balance Experience; Oak-Ridge Y-12 Plant.

47. Steele, R.S. Jr. and Babelay, E.F. Jr., Rotor Testing in FY 1981; Work performed at the Oak Ridge Y-12 Plant operated by Union Carbide Corporation, Nuclear Division, under contract W-7405-eng-26.

48. Steele, R.S. Jr. Babelay, E.F. Jr. and Sutton B.J., Oak Ridge Flywheel Evaluation Laboratory Annual Report; (October 1, 1979 - September 30, 1980), under U.S. Government Contract W-7405-eng-26.

49. Steele, R.S., Flywheel Testing and Evaluation; CRM 1982.

50. Stiffler, A. K., Pressurized Oil Squeeze Film Dampers; Journal of Lubrication Technology, Trans. of the ASME, Vol. 102, Jan. 1982, pp. 41-47.

51. Tessarzik, J.M. and Badgley R.H., Experimental Evaluation of the Exact Point-Speed and Least-Squares Procedures for Flexible Rotor Balancing by the Influence Coefficient Method; Journal of Engineering for Industry, Trans. ASME, Vol. 96, Series B, No. 2, May 1974, pp. 633-643.

52. Thomson, W.T., Younger F.C. and Gordon, H.S., Whirl Stability of the Pendulously Supported Flywheel System; ASME Journal of Applied Mechanics, Vol. 99, No. 2, June 1977, pp. 322-328.

53. Wells, D.A., Theory and Problems of Langragian dynamics; McGraw-Hill Book Company, Schaum's Outline Series, ISBN 07-069258-0, pp. 234-241.